International Journal of Heat and Mass Transfer 135 (2019) 1130–1151

Contents lists available at ScienceDirect

International Journal of Heat and Mass Transfer

journal homepage: www.elsevier.com/locate/ijhmt

Computation and physical explanation of the thermo-fluid-dynamics of natural convection around heated inclined plates with inclination varying from horizontal to vertical

Abhijit Guha *, Akshat Jain, Kaustav Pradhan

Mechanical Engineering Department, Indian Institute of Technology Kharagpur, Kharagpur 721302, India

ARTICLE INFO

Article history:
Received 12 July 2018
Received in revised form 2 January 2019
Accepted 11 January 2019

Keywords:
Natural convection
Inclined plates
CFD
Buoyant plume
Heat transfer

ABSTRACT

The paper invokes the power of computational fluid dynamics (CFD) for accurate determination of the detailed thermo-fluid-dynamics of natural convective flow around heated inclined plates, with an extensive experimental validation of the computed heat transfer results. The study provides fundamental physical insight through a comprehensive understanding of the behaviour of the contours of velocity, temperature and pressure as a function of inclination angle over the entire range from the vertical ($\gamma = 90^\circ$) to the horizontal ($\gamma = 0^\circ$). In particular, the present study documents, for the first time, qualitative and quantitative behaviour of the lift-off point at which the natural convective boundary layer converts into a free plume. Similarly, the details of the spatial evolution of the velocity profile and temperature profile in the plume as a function of the inclination angle of the plate are determined for the first time. It is shown how the relative importance of indirect pressure difference and direct buoyancy, as mechanisms of natural convection, changes as the inclination angle is gradually altered from the horizontal to the vertical. Through accurate computation (and ingenious representation) of the velocity, temperature and pressure fields at small intervals of the inclination angle, the subtle and complex thermo-fluid-dynamics in near-horizontal configurations is revealed. It is shown that the non-dimensional lift-off distance changes from 0.5 (middle of the plate) to 0.9816 (nearly the trailing edge) as the angle of inclination is changed from 0° to 15°. It is established that as the inclination angle is increased gradually from the horizontal position, the value of average Nusselt number $\overline{Nu}$ initially decreases slightly, passes through a minimum point and then onward increases continuously up to the vertical position of the plate.

1. Introduction

In a few recent papers the power of computational fluid dynamics (CFD) was invoked to obtain accurate solutions of natural convective flow above a heated horizontal plate [1], natural convection around a heated vertical plate [2] and mixed convection above a heated rotating disc [3]. In addition to obtaining accurate computation of the heat transfer rate, a major objective of these papers was to establish detailed fundamental physical understanding of the thermo-fluid-dynamics which is difficult to be obtained through other methods of investigation such as analytical or experimental. This spirit of CFD investigation is applied in the present paper to reveal the fine details of the thermo-fluid-dynamics of natural convective flow around inclined heated plates as the inclination of the plate is systematically varied from the horizontal to the vertical configuration. A complementary benefit of the computed results is that the previous work on the subject-matter, including a recently developed unified integral theory [4], can be put in perspective.

Natural convective flow is set up in a fluid due to density gradients that are in turn developed due to temperature differences in the fluid. Heat transfer by natural convection is an important physical phenomenon and is often encountered in engineering devices such as electronic equipments and nuclear reactors. Heated channel configurations which are cooled by natural convection are found in electronic cabinets containing circuit cards which are aligned in vertical or inclined arrays, with channels between each card [5]. Natural convection flows adjacent to plate-like geometries are of interest in a number of industrial applications such as the heat treatment of materials travelling between a feed roll and a wind-up roll or on conveyor belts, the hot extrusion of steel, the

* Corresponding author.
E-mail address: a.guha@mech.iitkgp.ac.in (A. Guha).

https://doi.org/10.1016/j.ijheatmasstransfer.2019.01.054
0017-9310/

Nomenclature

c_p	specific heat capacity (J/kg K)
Gr_L	Grashof number defined as $\rho_\infty^2 g\beta(T_w - T_\infty)L^3/\mu^2$
Gr_x	local Grashof number defined as $\rho_\infty^2 g\beta(T_w - T_\infty)x^3/\mu^2$
g	acceleration due to gravity (m/s^2)
h_x	local convective heat transfer coefficient (W/m^{2}K)
$\bar{h}$	average convective heat transfer coefficient (W/m^{2}K)
k	thermal conductivity (W/mK)
L	length of plate (m)
Nu_x	local Nusselt number defined as $h_x x/k$
$\overline{Nu}$	average Nusselt number defined as $\bar{h}L/k$
Pr	Prandtl number defined as $\mu c_p/k$
p	static pressure (Pa)
p_∞	ambient pressure (Pa)
Q	total surface heat flux (W)
q_x	local surface heat flux along the heated side of plate (W/m^2)
Ra_L	Rayleigh number defined as Gr_LPr
Ra_x	local Rayleigh number defined as Gr_xPr
T	fluid temperature (K)
T_w	temperature of the heated surface (K)
T_∞	ambient temperature (K)
t_P	thickness of plate (m)
u	component of velocity along the plate (m/s)
V_Y	component of velocity along Y-direction (m/s)
v	component of velocity normal to the plate (m/s)
$\vec{v}$	velocity vector
X	horizontal co-ordinate with origin at left (or trailing) edge of the heated side of the plate
x	co-ordinate along the plate with origin at right (or leading) edge of the heated side of the plate
$\bar{x}$	non-dimensional x coordinate defined as x/L
$\bar{x}_{lift-off}$	non-dimensional lift-off distance
$\bar{x}_{q_{x,\min}}$	non-dimensional minimum wall heat flux point
Y	vertical co-ordinate with origin at left (or trailing) edge of the heated side of the plate
y	co-ordinate normal to the plate with origin at right (or leading) edge of the heated side of the plate
$\bar{y}$	non-dimensional y coordinate defined as y/L

Greek symbols

β	coefficient of thermal expansion (/K)
γ	inclination angle (degree)
μ	dynamic viscosity (Pa-s)
ρ	density (kg/m^3)
ρ_∞	density at temperature T_∞ (kg/m^3)

lamination and melt-spinning processes in the extrusion of polymers, etc. [6]. Therefore, the phenomenon of natural convection adjacent to flat plates and other geometries has been extensively studied considering different surface thermal conditions.

Similarity analysis of natural convection past a semi-infinite isothermally heated vertical plate is now a standard element of all books on convection [7–10]. Laminar natural convection on a vertical plate has been studied by experiments [11–14], similarity theory [15] and integral theories [16]. Recently, Guha and Nayek [2] studied in great detail the thermo-fluid-dynamics of natural convection past a finite vertical plate. The effect of implementing the routinely used boundary condition $u = 0$ at $x = 0$ in the similarity and integral theories is investigated in Ref. [2], and an important discovery has been made. It is found that the streamline pattern is drastically altered and the Nusselt number is significantly affected by the usual boundary condition imposed at $x = 0$. (The same boundary condition continues to be assumed in related theoretical analyses, even in recent publications, without any introspection.) As compared to the measured values, the similarity theory underpredicts the Nusselt number for fluids having low Prandtl number whereas it overpredicts the Nusselt number for fluids having high Prandtl number. The CFD results, with proper boundary conditions, bring the theoretical analysis closer to experiments for both low and high values of the Prandtl number. If x and y are respectively the co-ordinates along and perpendicular to the plate, the boundary layer type theories (such as similarity and integral theories) for natural convection around a semi-infinite, isothermally heated vertical plate assume that there is no pressure gradient along the surface ($\partial(p - p_\infty)/\partial x = 0$) and perpendicular to the plate ($\partial p/\partial y = 0$), where p is the local static pressure and p_∞ is the ambient (quiescent) pressure. (Present computations show that these two conditions are approximately true in the central portion of a finite vertical plate.) The convective motion of fluid is almost entirely caused directly by the buoyancy force.

The direct buoyancy force, however, has no component along the surface of a horizontal plate. The buoyancy force, on the other hand, generates a pressure gradient along the surface, which, in turn, drives the natural convective flow above a heated horizontal plate. Unlike the boundary layer that forms due to forced convection, the boundary layer on a horizontal plate due to natural convection is such that $\partial p/\partial y \neq 0$ and $\partial p/\partial x$ cannot be neglected inside the boundary layer (even when $\partial p_\infty/\partial x$ is zero). The mechanism of natural convection above a horizontal plate is thus quite different from that around a vertical plate, and was termed as 'indirect natural convection' by Schlichting and Gersten [10] due to the nature of its generation. A quantitative mathematical theory of 'indirect natural convection' can be discerned from the work of Guha and Pradhan [4]. Using the Boussinesq approximation, the y-momentum equation in the boundary layer formulation may be integrated from a given location y to the edge of boundary layer ($y = \delta$) to give $p - p_\infty = -\rho_\infty g\beta\int_y^\delta (T - T_\infty)\,dy$. This shows that the static pressure on the surface of a heated horizontal plate is below the ambient pressure and therefore $\partial p/\partial y \neq 0$. Moreover, differentiation of the preceding equation with respect to x shows mathematically how the buoyancy gives rise to an induced non-zero pressure gradient along the surface causing 'indirect natural convection': $-\frac{1}{\rho_\infty}\frac{\partial p}{\partial x} = g\beta\frac{\partial}{\partial x}\int_y^\delta (T - T_\infty)\,dy$ (for horizontal plate and quiescent atmosphere $\partial p_\infty/\partial x = 0$).

Natural convection over a heated horizontal surface has been studied using similarity theory [17], integral theory [18] and experiments [19]. According to Schlichting and Gersten [10], Stewartson [20] was one of the pioneers to show the existence of this type of boundary layer flow. Stewartson [20] considered an isothermal semi-infinite flat plate and derived the self-similar velocity and temperature profiles for the case of both hot and cold surface facing upwards. Later on, Gill et al. [21] interpreted the inconsistency of this solution and showed the existence of similarity solution with either hot surface facing upwards or cold surface facing downwards. A similarity analysis has been performed by Rotem and Claassen [19] for natural convection over a heated semi-infinite horizontal plate; the reference also includes experimental data and coloured visualization pictures. Guha and Sengupta [1] presented a comprehensive analysis of the effects of the finiteness of a heated horizontal plate on the thermo-fluid-dynamics of natural convection above it. The 3-D CFD simulations there are coordinated to clearly reveal the separate and combined effects of three important aspects of finiteness: the presence of

leading edges, the presence of planform centre and the presence of physical corners in the planform. The presence of physical corners is related to several significant aspects of the solution - the conversion of in-plane velocity to out-of-plane velocity near the diagonals, the star-like non-uniform distribution of surface heat flux on heated planforms, the three-dimensionality of the temperature field and the complex spatial structure of the velocity iso-surfaces. A generic theoretical correlation for the Nusselt number is mathematically deduced for the averaged surface heat flux for various rectangular surfaces (with aspect ratio ϕ varying in the range $1 \leqslant \phi < \infty$) over a wide range of Grashof number. It is shown that two parameters based on the length scales are required to adequately represent the effects of finiteness of a rectangular planform on the natural convection heat transfer: Θ (ratio of surface area and perimeter) and ϕ (aspect ratio) are used in the deduced correlation [1], $Nu^* = C_S[\phi/(\phi+1)]^{1/10} Gr^{*1/5}$, where the Nusselt number Nu^* and Grashof number Gr^* are defined with the generic length scale Θ, and C_S is a function of Prandtl number and is derivable from the similarity theory. Powerful numerical visualizations [1], obtained by post-processing of the CFD solutions, capture and present the quantitative details of the three-dimensionality of the velocity and temperature fields in relation to the geometric features of a finite planform; the completeness of this knowledge will be difficult to achieve through any other line of investigation – experimental or theoretical. Apart from these, several other studies pertaining to natural convection of different types of fluids (non-Newtonian fluid, nanofluid, etc.) above horizontal surfaces may be found in Refs. [22–25].

Many engineering heat transfer applications involve cases of natural convection where the surface heating conditions are non-uniform [26]. Solutions for vertical plates with non-uniform surface temperature are given in [8,26]. For horizontal plates, Chen et al. [27] solved integro-differential equations by finite difference method for two values of the Prandtl number - 0.7 and 7. In a recent study [17], similarity theories have been developed for natural convection in fluids with arbitrary Prandtl number on horizontal surfaces for generic power law variations in wall temperature or wall heat flux. Another study [18] develops the corresponding integral theories giving explicit analytical expressions for the Nusselt number as functions of Grashof number, Prandtl number and indices of non-uniform heating. This reference also contains a good discussion on the role of Prandtl number in natural convective flow. Prandtl number determines the ratio of the thickness of velocity boundary layer (δ_V) and that of thermal boundary layer (δ_T). In the case of forced convection heat transfer [7,10,28], it is found that $\delta_V/\delta_T \sim \mathrm{Pr}^{1/2}$ for fluids with low Prandtl number and $\delta_V/\delta_T \sim \mathrm{Pr}^{1/3}$ for fluids with medium or high Prandtl number. Therefore, for forced convection, $\delta_V < \delta_T$ when $\mathrm{Pr} < 1$, $\delta_V \sim \delta_T$ when $\mathrm{Pr} \sim 1$, $\delta_V > \delta_T$ when $\mathrm{Pr} > 1$. This behaviour is consistent with the definition of Prandtl number which is defined as the ratio of the momentum and thermal diffusivities. It may be construed that this role of Prandtl number remains the same for the case of natural convection also. A comment made in reference [7,p525] ("$\delta_V \approx \delta_T$ only if $\mathrm{Pr} \approx 1$"), has drawn our attention to this possible implication. Ghiaasiaan [29,p278] has also commented that the relative thickness of the two boundary layers follows the same trend in forced and natural convection. An opposite qualitative argument could also be formed that, since the two boundary layers are coupled in natural convection, they would be of similar thickness at all Prandtl numbers (as may be implied in Fig. 10.16 in Schlichting & Gersten [10,p281]). In order to settle this issue qualitatively and quantitatively, detailed calculations have been performed in Ref. [18] with the help of the recently developed similarity theory for natural convection on horizontal plates [17]. These calculations establish that, in natural convection, the two boundary layers are of comparable thickness if $\mathrm{Pr} \leqslant 1$ or $\mathrm{Pr} \approx 1$. It is only when the Prandtl number is large ($\mathrm{Pr} > 1$) that the velocity boundary layer is thicker than the thermal boundary layer. In natural convection, the velocity boundary layer is never less thick than the thermal boundary layer since the fluid is set into motion due to thermal effects (buoyancy). The velocity boundary layer can, however, become thicker than the thermal boundary layer, when the Prandtl number is very large, because natural convective velocity may persist away from the wall due to shear force and inertia (even when buoyancy is absent).

In contrast to the extensive literature that exists for natural convection over horizontal or vertical surfaces, the literature available for inclined surfaces is rather limited. Rich [30] performed experiments for the natural convection of air adjacent to isothermal inclined surfaces with inclination angles in the range $50^\circ < \gamma < 90^\circ$. Extensive experiments of natural convective flow of air around heated inclined plates ($15^\circ < \gamma < 90^\circ$) were performed by Sang-Urai [31] to determine the temperature distribution and convective heat transfer coefficient. Vliet [32] gave experimental results for the natural convective flow of water past inclined surfaces ($30^\circ < \gamma < 85^\circ$) subjected to constant heat flux. Since natural convection on inclined surfaces does not admit similarity solution, they [30,32] tried to relate the heat transfer results on inclined surfaces to the limiting cases of vertical and horizontal surfaces by using the component of gravity along the inclined surface for calculating the Grashof number in their analysis. A few studies have derived the non-similar boundary layer equations for natural convection on an inclined surface and solved those using elaborate numerical techniques [27,33]. Saha et al. [34] performed scaling analysis of natural convection adjacent to inclined plates subjected to sudden and ramp heating boundary conditions. Corcione et al. [35] considered natural convection on inclined plates where both sides of the plate are maintained at the same temperature. The finest grid structure in this study was 100×400, and the physically interesting (and computationally challenging) range of near-horizontal configurations ($0^\circ \leqslant \gamma < 15^\circ$) were not considered.

While it has been possible to develop self-similarity theory for vertical plate ($\gamma = 90^\circ$) and horizontal plate ($\gamma = 0^\circ$), the flow solutions for all other inclination angles are found to be non-similar. Similarity theories show that the Nusselt number varies as the one-fourth power of Grashof number for natural convection on an isothermal vertical surface ($Nu_x \propto Gr_x^{1/4}$) while it varies as the one-fifth power of Grashof number ($Nu_x \propto Gr_x^{1/5}$) for isothermal horizontal surfaces. Since the natural convection mechanisms for both vertical and horizontal configurations are operative in case of inclined surfaces, the development of a closed-form solution for the Nusselt number, which will reduce to the known solutions in the two limits of horizontal and vertical surfaces, is difficult. Recently, Guha and Pradhan [4] applied the integral method to formulate a set of simple generic equations that represents natural convection on horizontal, inclined and vertical surfaces subjected to arbitrary variation in wall temperature or surface heat flux for a wide range of parameters ($10^3 \leqslant Gr \leqslant 10^7$, $0.01 \leqslant \mathrm{Pr} \leqslant 100$ and $0^\circ \leqslant \gamma \leqslant 90^\circ$). The paper also provides algebraic expressions for Nusselt number as explicit functions of Grashof number, Prandtl number and inclination angle for both uniform surface temperature and uniform surface heat flux. The relations are mathematically deduced for the special cases of vertical and horizontal plates, with optimized profiles for velocity and temperature within the boundary layer. Guha and Pradhan [4] quantified, for the first time, the relative contribution of the horizontal and vertical mechanisms of natural convection on an inclined surface. By integrating the x -momentum equation in the boundary layer within the limits $y = 0$ and $y = \delta$, They showed that the momentum integral equation becomes

$$\frac{d}{dx}\int_0^\delta u^2 dy = -\frac{1}{\rho_\infty}\int_0^\delta \frac{\partial(p-p_\infty)}{\partial x}dy + g\beta\sin\gamma\int_0^\delta (T-T_\infty)dy - \upsilon\left.\frac{\partial u}{\partial y}\right|_{y=0} \quad (1)$$

inertia; indirect pressure difference; direct buoyancy; viscous

The first term in the RHS of Eq. (1) represents the 'induced' or 'indirect pressure gradient' producing convective flow parallel to the solid surface, in which the gradient of gauge pressure $\partial(p-p_\infty)/\partial x$ is deduced as $\frac{\partial(p-p_\infty)}{\partial x} = -\rho_\infty g\beta\cos\gamma\frac{\partial}{\partial x}\left((T_w-T_\infty)\frac{\delta}{\chi+1}\left(1-\frac{y}{\delta}\right)^{\chi+1}\right)$, where χ is the order of the polynomial representing the temperature profile within the boundary layer. The second term in the RHS of Eq. (1) is the component of buoyancy force acting along the inclined surface. This is a measure of the 'direct buoyancy' causing convective flow along the surface. For a horizontal surface ($\gamma = 0^\circ$), the 'direct buoyancy' vanishes and the convective flow in the horizontal direction is driven by the 'indirect pressure difference' alone. On the other hand, for a vertical surface ($\gamma = 90^\circ$), the 'indirect pressure difference' vanishes and the flow is driven along the surface only by the 'direct buoyancy'. For an inclined surface, both mechanisms are operative.

All integral and similarity analyses are restricted by some assumptions: (i) the plate is semi-infinite, (ii) the boundary layer equations are valid, (iii) there is no buoyant plume, (iv) the plate thickness is negligible, and (v) the flow occurs on only one side of the plate. In order to ensure self-similarity, sometimes, non-physical boundary conditions may also be used [2]. Since a practical plate is of finite length and thickness, and natural convective flow may be induced on both sides of the plate, with a deviation from boundary-layer type of flow (such as formation of buoyant plume), the above assumptions may lead to inability of the solution in capturing all the intricate features of the temperature and velocity fields. In the present paper, the power of computational fluid dynamics (CFD) is invoked to develop a thorough physical understanding of the interaction of the horizontal and vertical mechanisms in the natural convective flow adjacent to a finite inclined plate, with an extensive experimental validation of the computed heat transfer results. The goal of the present study, however, is not merely the calculation of the Nusselt number. It provides fundamental physical insight through a comprehensive understanding of the behaviour of the contours of velocity, temperature and pressure as a function of inclination angle over the entire range from the vertical ($\gamma = 90^\circ$) to the horizontal ($\gamma = 0^\circ$). In particular, the present study documents, for the first time, qualitative and quantitative behaviour of the lift-off point at which the natural convective boundary layer converts into a free plume. The subtle and complex fluid dynamics and heat transfer in the range $0^\circ \leqslant \gamma \leqslant 15^\circ$ are revealed.

A systematic method is employed for all CFD simulations. The actual quantitative dependence of the fluid dynamics and heat transfer on the inclination angle has been determined here from a large number of separate computational fluid dynamic (CFD) simulations, each run to a high degree of convergence (the 'scaled' residual for all conserved variables is set as 10^{-6} which is considerably smaller than what is normally set in much of the reported CFD work). A large number of grid points (up to about 0.9 million) and double precision arithmetic are used to obtain high precision of the computed results. Great care is taken here to ensure grid independence and domain independence of the presented solutions. Moreover, second order accurate discretization schemes are used. This comprehensiveness and precision have helped us to formulate generic principles and identify subtle physical mechanisms.

2. Mathematical formulation

The present study considers laminar natural convective flow around a heated plate inclined at an angle γ to the horizontal (Fig. 1). The Navier-Stokes equations expressed in a Cartesian coordinate system are the governing equations for the above-mentioned flow system and are given below:

$$\frac{\partial\rho}{\partial t} + \vec{\nabla}.(\rho\vec{v}) = 0 \quad (2)$$

$$\frac{\partial(\rho\vec{v})}{\partial t} + \vec{\nabla}.(\rho\vec{v}\vec{v}) = -\vec{\nabla}p + \vec{\nabla}.\left(\mu\vec{\nabla}\vec{v} + \mu\vec{\nabla}\vec{v}^T - \frac{2}{3}\mu\vec{\nabla}.\vec{v}\right) + \rho\vec{g} \quad (3)$$

$$\frac{\partial(\rho T)}{\partial t} + \vec{\nabla}.(\rho\vec{v}T) = \vec{\nabla}.\left(\frac{k}{c_p}\vec{\nabla}T\right) + \Phi \quad (4)$$

In Eqs. (2)-(4), $\vec{v}$ denotes the velocity vector, p is the static pressure and T is the temperature of the fluid. ρ, μ, c_p and k are respectively the density, dynamic viscosity, specific heat capacity at constant pressure and thermal conductivity of the fluid. $\vec{g}$ is the gravity vector. Φ in Eq. (4) represents the viscous dissipation term which is usually small [36] for natural convection and hence, is neglected in the present study. The final steady-state is obtained as the limiting converged solution of an unsteady process (i.e. when the unsteady terms in Eqs. (2)-(4) tend to zero). All the thermo-physical properties of the fluid like dynamic viscosity, specific heat capacity and thermal conductivity, except the density in the body force term (last term on right hand side of Eq. (3)), are considered to be constant. The Boussinesq approximation, which considers a linear variation of density with temperature rise, is adopted here for the variation of density in the body force term. According to the Boussinesq approximation,

$$\rho = \rho_\infty[1 - \beta(T - T_\infty)] \quad (5)$$

where β is the thermal expansion coefficient of the fluid, T_∞ and ρ_∞ are respectively the temperature and density of the quiescent fluid far away from the heated plate.

A two-dimensional analysis is performed here for which the width of the plate perpendicular to the plane of the paper is assumed infinite. The x -coordinate is taken along the plate and the y-coordinate is measured normal to the plate (Fig. 1). The origin of the co-ordinate system is taken at point O which is the lowest point on the heated surface (right-most point for horizontal configuration). The velocity component along the x-direction (along the plate) is u. The velocity component along the y-direction (normal to the plate, pointing away from the plate on the heated side of the plate) is v. It is to be noted that, with respect to any globally fixed co-ordinate system, the co-ordinate axes x

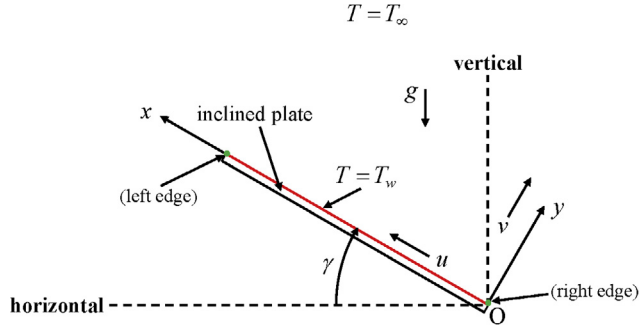

Fig. 1. A physical model and coordinate system for the analysis of natural convection around an isothermally heated inclined plate.

and y (and hence u and v) rotate with the plate as its inclination is varied. Gravity $\vec{g}$ acts vertically downwards, which is in the negative y-direction for the horizontal plate orientation ($\gamma = 0^\circ$).

The heat transfer results in the study of natural convection adjacent to a flat plate are usually presented in terms of the Nusselt number (Nu) or the convective heat transfer coefficient (h). The local heat flux at any position (x) along the plate is computed using the following expression:

$$q_x = -k\left(\frac{\partial T}{\partial y}\right)_{y=0} \tag{6}$$

The local convection heat transfer coefficient h_x is given by:

$$h_x = \frac{q_x}{(T_w - T_\infty)} \tag{7}$$

The local Nusselt number (Nu_x) is evaluated from the local convective heat transfer coefficient (h_x) according to the following expression:

$$Nu_x = \frac{h_x x}{k} \tag{8}$$

where x is the distance along the plate from the leading (right) edge and k is the thermal conductivity of the fluid. The average Nusselt number ($\overline{Nu}$) is evaluated from the following expression:

$$\overline{Nu} = \frac{\bar{h}L}{k} \tag{9}$$

where L is the length of the plate and $\bar{h}$ is the average convective heat transfer coefficient that is calculated from h_x using the following expression:

$$\bar{h} = \frac{1}{L}\int_0^L h_x dx \tag{10}$$

Taking cue from previous studies for natural convective flow, we define the following dimensionless parameters:

Grashof number:

$$Gr_L = \frac{\rho_\infty^2 g\beta(T_w - T_\infty)L^3}{\mu^2} \tag{11}$$

Prandtl number:

$$\mathrm{Pr} = \frac{\mu c_p}{k} \tag{12}$$

Rayleigh number:

$$Ra_L = Gr_L \mathrm{Pr} = \frac{\rho_\infty^2 g\beta(T_w - T_\infty)c_p L^3}{\mu k} \tag{13}$$

3. Computational fluid dynamic simulations

The governing equations for natural convective flow (Eqs. (2)-(4)) around an inclined plate are solved using a commercial finite-volume based CFD solver Fluent [37]. Two-dimensional simulations are performed with the assumption that the dimension of the plate in the direction perpendicular to the plane shown in Fig. 1 is infinitely large. A structured mesh is constructed for the chosen computational domain using ANSYS Meshing and a systematic grid independence study is performed.

3.1. Geometry, grid and boundary conditions

A flat plate of length L and thickness t_P ($= L/100$) is considered in the present study. It is assumed that one side of the plate is maintained at a temperature T_w ($> T_\infty$) while the other three sides are insulated (i.e. adiabatic condition is maintained there). In their experiments, Rich [30], Sang-Urai [31] and Vliet [32] used an insulated surface ($q_w = 0$) for the side of the inclined plate opposite to the heated side. We have also used the adiabatic ($q_w = 0$) boundary condition for that side of the plate. However, there is no explicit mention of the condition on the two edges along the thickness (t_P) of the plate used in the experiments. We have used the adiabatic condition there so that it does not affect the total heat transfer from the plate (and hence the Nusselt number calculations). The no-slip and no-penetration boundary conditions are applied on all the four sides of the plate. Mathematically, the boundary conditions for the four sides of the plate may be listed as follows:

Heated side of plate:

$$\text{At } y = 0, 0 \leqslant x \leqslant L : u = v = 0,\ T = T_w. \tag{14}$$

Other three sides of plate:

$$\text{At } x = 0,\ -t_P \leqslant y \leqslant 0 : u = v = 0,\ q_w = 0. \tag{15}$$

$$\text{At } x = L,\ -t_P \leqslant y \leqslant 0 : u = v = 0,\ q_w = 0. \tag{16}$$

$$\text{At } y = -t_P,\ 0 \leqslant x \leqslant L : u = v = 0,\ q_w = 0. \tag{17}$$

Our previous and present computational experience shows that a boundary layer also develops along the adiabatic length of the plate. There is also entrainment of comparable magnitude on the two sides of the free plume. For these reasons, the plate is located at the centre of the rectangular computational domain (Fig. 2). For non-vertical orientations, the isothermal side of the plate is placed upward.

Fig. 2 shows that the computational domain is notionally divided into eight sub-domains, viz., S1, S2,. . ., S8, for having control over appropriate grid structure and for the ease of future reference. The "pressure outlet" boundary condition available in Fluent is applied at the periphery of the overall computational domain. In Fluent, when the gravitational acceleration is activated in the simulation of incompressible flow, the static pressure p at a point is re-defined as $p' = p - \rho_\infty \vec{g}\cdot\vec{r}$ [37], where ρ_∞ is the ambient density of the fluid (which is assumed constant), $\vec{g}$ is the gravitational acceleration and $\vec{r}$ is the position vector. The "pressure outlet" boundary condition feature requires the specification of the re-defined (gauge) static pressure p'. Since the hydrostatic pressure is already contained in the modified pressure p', setting $p' = 0$ on all the boundaries of the overall computational domain automatically sets $p = p_\infty$ there, p_∞ being the ambient pressure that varies in the direction of gravity according to the hydrostatic equation.

Our experience shows that the computational domain must be selected carefully for accurate simulations of natural convection. The size of the computational domain is selected (through a domain independence study described later) such that all flow variables attain their quiescent values asymptotically. For high level of precision, a very fine grid structure is adopted after a careful grid independence study (described below). As an example of the systematic method followed here, Fig. 3 shows the fine grid, containing 882,616 computational cells, for a vertical plate ($\gamma = 90^\circ$) and the corresponding contours of the u -velocity at $Gr_L = 10^6$ and $\mathrm{Pr} = 0.7$. The position and size of the plate are identified by a white line in Fig. 3; this also indicates relative size of the computational domain. The contour plot is physically satisfying as the above-mentioned criteria of a good flow solution are fulfilled. For example, it is seen that the u-velocity has asymptotically reduced to practically zero value long before the left and right boundaries of the computational domain. Similarly, the u-velocity is practically zero at the left and right portions of the top and bottom boundaries. This indicates that the domain is sufficiently large for the fluid to attain quiescent condition at the domain boundaries. The velocity contour in Fig. 3 also shows that

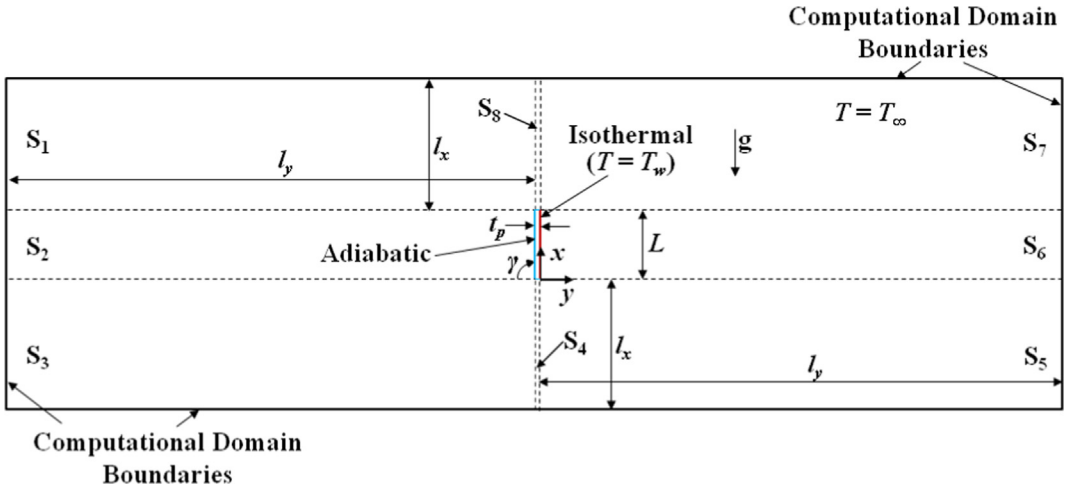

Fig. 2. The schematic details of the computational domain for $\gamma = 90^{\circ}$ used in the present CFD analysis.

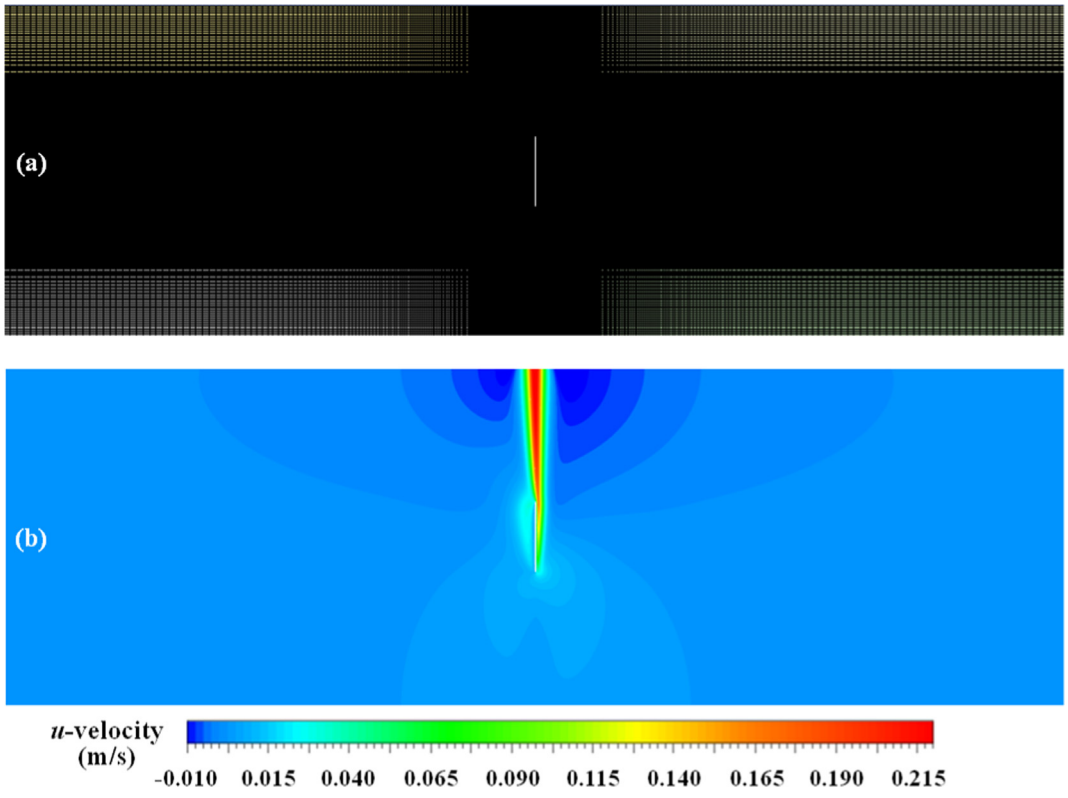

Fig. 3. Fine grid structure and the corresponding velocity contours (for $Gr_L = 10^6$ and Pr = 0.7) in the computational domain for $\gamma = 90^{\circ}$. (The position and size of the plate are identified by a white line; right hand side is isothermal, other three sides are adiabatic.)

there is only upward entrainment (at comparatively low flux) through the bottom boundary. On the top boundary, there exists both upward efflux (the plume) as well as downward entrainment of fluid. The main natural convective boundary layer forms on the right side; however, Fig. 3 shows that there is a small movement of the fluid on the left side of the plate as well, as a small fraction of the entrained fluid at the leading edge of the plate spills over to the left side. The flow field and the temperature field on the left and right sides of the plate are not the same (left-right asymmetry). As the buoyant plume leaves the trailing edge of the plate, it bends over the plate due to the left-right asymmetry and due to the finite thickness of the plate.

In the present study, we have considered laminar flow. The fluid flow over an inclined plate due to natural convection becomes unstable above a critical value of Ra_L. In case of vertical flat plate the critical value of Ra_L is 9×10^9 [38,39]. Llyod et al. [40] conducted experiments on variously shaped (rectangular, circular and right-triangular) finite horizontal surfaces from which they concluded that transition from laminar to turbulent flow takes place at about $Gr\mathrm{Pr} = 8 \times 10^6$. The present theoretical study with parametric variation in the inclination angle γ is conducted at $Gr_L = 10^6$ and Pr = 0.7 so that the flow remains laminar above the plate. The following constant values of the parameters are used

to obtain the above-mentioned values of the non-dimensional parameters: $T_w = 325$ K, $T_\infty = 300$ K, $\rho_\infty = 1.1614$ kg/m^3, $\beta = 0.00333$ K^{-1}, $\mu = 3.32 \times 10^{-5}$ Pa − s, $k = 0.04773$ W/(mK), $c_p = 1007$ J/(kgK) and $L = 0.1$ m. With increasing height from the trailing (left) edge of the inclined plate, the local Reynolds number Re_x ($\equiv \rho_\infty u\delta/\mu$) of the buoyant plume created by the heated plate increases due to fluid entrainment (δ is the local width of the plume at any x). The value of Re_x should not exceed 10^4 for the flow in the jet to remain laminar [41]. This condition is well satisfied here. Later, for experimental verification, several additional CFD simulations are run at various values of Rayleigh number to match corresponding experimental conditions available in the literature (Section 4.4).

3.2. Numerical schemes

The governing Eqs. (2)–(4) are solved numerically using the pressure-based solver available in FLUENT. All transport equations are discretized to be second order accurate in space. The second order upwind scheme provided in Fluent is used for the discretization of the advection terms, while the central difference scheme is used for discretizing the diffusion terms in the momentum and energy equations. The second order scheme is employed for the discretization of pressure. The SIMPLE algorithm is used for pressure-velocity coupling. Under-relaxation factors are suitably employed such that numerical instabilities are avoided but computational time does not increase excessively. A segregated implicit [42] solver is used to solve the resulting system of discretized equations. The solver uses a time-marching technique [43,44] to obtain a steady-state solution as the limiting process of an unsteady simulation. In all simulations, a solution is said to be converged if the scaled residuals reach 10^{-6} for all the governing equations (which is considerably smaller than what is normally set in much of the reported CFD work). A large number of grid points and double precision arithmetic are used to obtain high precision of the computed results.

3.3. Domain independence test

We have performed separate domain independence tests for the various inclination angles considered in the present work. However, here we present the results at only $\gamma = 45^\circ$ for brevity, as an illustrative example of the adopted procedure. In order to perform a systematic domain independence test, we have used the same grid structure for all the domains.

Table 1 shows that as the size of the computational domain (in terms of l_x and l_y) is systematically increased, the values of the computed average Nusselt number $\overline{Nu}$ uniformly converge. Between domains D2 and D3, there is no difference in $\overline{Nu}$ up to the second decimal place and the relative change in the value is less than 0.01%. Accordingly, domain D2 is considered adequate for $\gamma = 45^\circ$ and is used for all subsequent simulations at $\gamma = 45^\circ$.

Following a similar procedure, separate domain independence tests are carried out at each angle of inclination, which specify the particular values of l_x and l_y that are appropriate for the particular angle of inclination. The size of the computational domain therefore varies according to the orientation of the plate.

Table 1
Results of the domain independence test for three computational domains at $\gamma = 45^\circ$ ($Gr_L = 10^6$, Pr = 0.7).

Name of the computational domain	l_x/L	l_y/L	$\overline{Nu}$
D1	2	2	14.7999
D2	4	4	14.8284
D3	8	8	14.8299

3.4. Grid independence test

A systematic grid independence study is reported below for an inclination angle of 45° and Pr = 0.7. Three grid structures are constructed—viz., "coarse", "medium" and "fine" — as shown in Table 2. The value of Δy_1 is progressively decreased as the grid is progressively refined from "coarse" to "fine." A non-uniform grid distribution (with $\Delta x_1 = \Delta y_1$ and geometric progression ratio of 1.02) is used in both x and y-directions so that the natural convective boundary layer is appropriately resolved, and at the same time, a large computational domain can be utilized so that the boundary conditions for the natural convective flow can be applied appropriately. The size of the grid is allowed to grow only up to set limits. Corresponding to the fine grid, there are 1020 grid points on the heated surface of the plate. Similarly, the flow fields around the plate corners are finely resolved as the minimum size of a computational element there is $\Delta y_1 \times \Delta y_1$.

Table 2 shows that as the grid size is systematically refined (following the method described above) from "coarse" to "fine", the values of the computed average Nusselt number $\overline{Nu}$ uniformly converge. Between the "medium" and "fine" grid structures for $Gr_L = 10^6$ (at which the parametric study for inclination angle is conducted in the present paper), there is no difference in $\overline{Nu}$ up to the second decimal place and the relative change in the value is less than 0.03%. Since for experimental validation of the computed results (given later in Section 4.4) the simulations need to be run at various values of Grashof number other than $Gr_L = 10^6$, we conducted additional grid independence tests at two other Grashof numbers, the results of which are also included in Table 2. The results demonstrate that the adopted computational methodology is robust. Although the "medium" grid would have been considered adequate on the basis of the grid independence data alone (Table 2), the "fine" grid with 799,784 computational elements is used for all subsequent simulations for $\gamma = 45^\circ$ for improved precision of computed results and quality of the flow visualization diagrams.

4. Results and discussion

CFD simulations are run for various combinations of the Grashof number and Prandtl number at various values of the inclination angle in the range $0^\circ \leqslant \gamma \leqslant 90^\circ$ for a thorough understanding of the thermo-fluid-dynamics of natural convection on a heated inclined plate. Comparisons are made with existing experimental

Table 2
Results of the grid independence test for three grid distributions in domain D2 ($\gamma = 45^\circ$, Pr = 0.7).

Grid distribution	First grid size adjacent to plate, Δy_1 (m)	Number of computational elements	$\overline{Nu}$		
			$Gr_L = 10^5$	$Gr_L = 10^6$	$Gr_L = 10^7$
Coarse	0.0001	394,272	8.9144	14.7911	25.3070
Medium	0.000075	489,804	8.9248	14.8243	25.3747
Fine	0.00005	799,784	8.9290	14.8284	25.3888

and theoretical results. For streamlining the discussion, the results are divided into a few subsections.

4.1. The physics of the natural convective boundary layer

In this section, the contours of velocity, temperature and pressure around an inclined plate obtained by the present simulations are shown for different values of the inclination angle ranging from the vertical ($\gamma = 90^\circ$) to the horizontal ($\gamma = 0^\circ$). It was shown in Guha and Pradhan [4] that for Pr $\sim$ 1, the natural convection mechanism for a vertical surface is the dominating factor for a large range of inclination angles except for near-horizontal configurations. With the above knowledge and due to representational convenience, here we have presented the results in two groups: $30^\circ \leqslant \gamma \leqslant 90^\circ$ and $0^\circ \leqslant \gamma \leqslant 15^\circ$.

The contours of velocity for $30^\circ \leqslant \gamma \leqslant 90^\circ$ are shown in Fig. 4. A boundary layer develops on the heated surface of the plate with convective velocities that decrease as the angle of inclination decreases from 90° to 30°. The finiteness of the size of the plate results in the formation of a buoyant plume that is found at the trailing edge of the plate for $30^\circ \leqslant \gamma \leqslant 90^\circ$. The plume-width at a specified distance above the trailing edge is found to increase as the inclination angle γ decreases. Moreover, for all values of γ shown in Fig. 4, as the vertical distance above the trailing edge of the plate increases, the plume-width increases due to entrainment of fluid from both sides. Although the natural convective boundary layer forms on the heated (right) side of the plate, a small movement of the fluid can be observed on the insulated (left) side of the plate as well. This may be attributed to the spilling over of a small fraction of the entrained fluid at the leading edge of the plate [2]. For $\gamma \leqslant 60^\circ$, a stagnation region starts developing on the insulated side of the plate. This region (dark blue colour) is found to expand considerably as the inclination decreases to 30°. Fig. 4 also shows that as the inclination angle decreases from 90° to 30°, the region around the inclined plate where the fluid is set into motion expands. Another interesting observation that can be made from Fig. 4 is that as the buoyant plume rises from the trailing edge of the plate, it bends; the degree of bending increases as the inclination angle decreases.

The contours of velocity for $0^\circ \leqslant \gamma \leqslant 15^\circ$ are shown in Fig. 5. Certain features of the velocity contour for this range of inclination angles remain similar to those observed in Fig. 4: (i) a boundary layer develops on the heated surface of the plate, (ii) a buoyant plume forms due to finiteness of the plate, with the plume-width increasing with vertical distance, and (iii) a stagnation region develops on the insulated side of the plate which shifts from near the leading (right) edge towards the centre of the plate as γ decreases from 15° to 0°. However, there are some mentionable differences in the flow physics at small inclination angle shown in Fig. 5. Firstly, the buoyant plume lifts off from the heated surface before the (trailing) left edge is reached; the location of detachment shifts toward the centre of the plate as the inclination angle decreases from 15° to 0°. Secondly, the convective velocities in the boundary layer near the plate decrease as the inclination angle decreases. Thirdly, a second boundary layer starts to develop from the left edge as the location of detachment of the buoyant plume shifts toward the centre of the plate. The length of this second boundary layer increases as γ decreases, to finally become equal to that of the initial boundary layer (that originating from the right edge) for $\gamma = 0^\circ$. Fourthly, the bending of the plume decreases as the inclination angle decreases from 15° to 0°; the plume is exactly vertical from the point of detachment for the horizontal case.

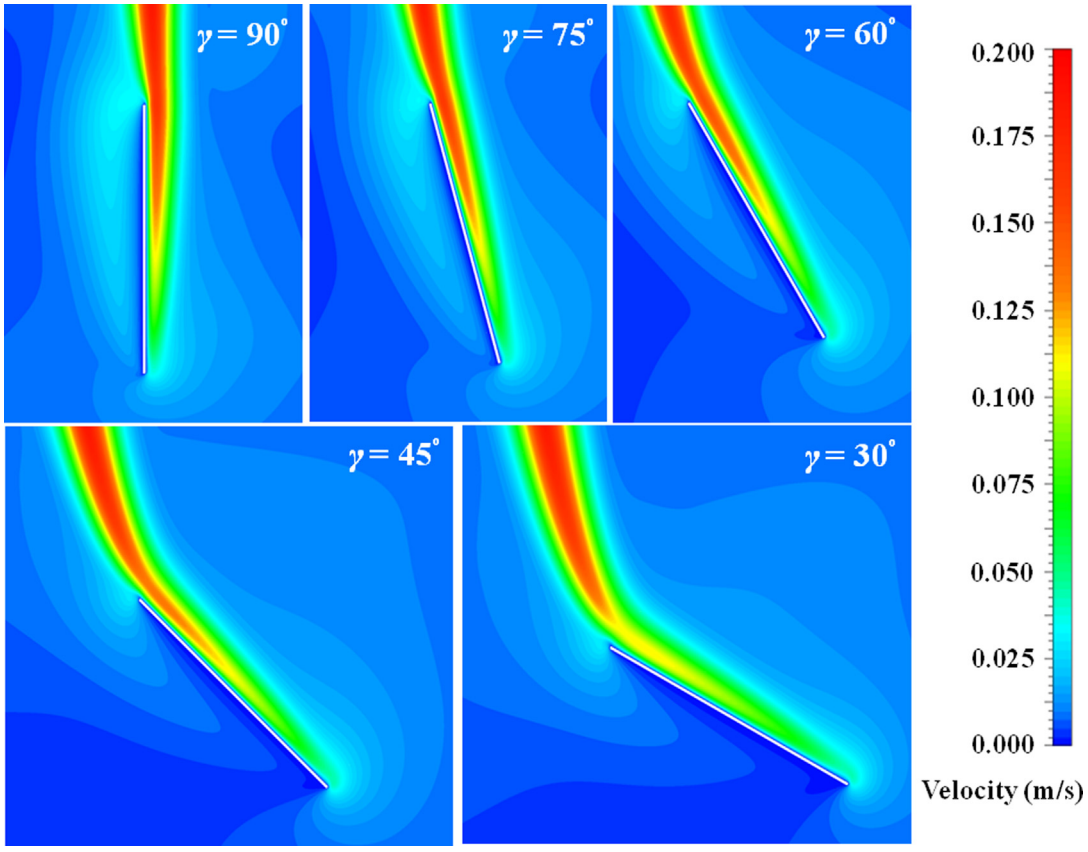

Fig. 4. Velocity contours adjacent to isothermally heated inclined plates at various inclinations of the plate in the range $30^\circ \leqslant \gamma \leqslant 90^\circ$. (Predictions of the present CFD simulations for Pr = 0.7 and $Gr_L = 10^6$ with $T_w - T_\infty = 25$ K.)

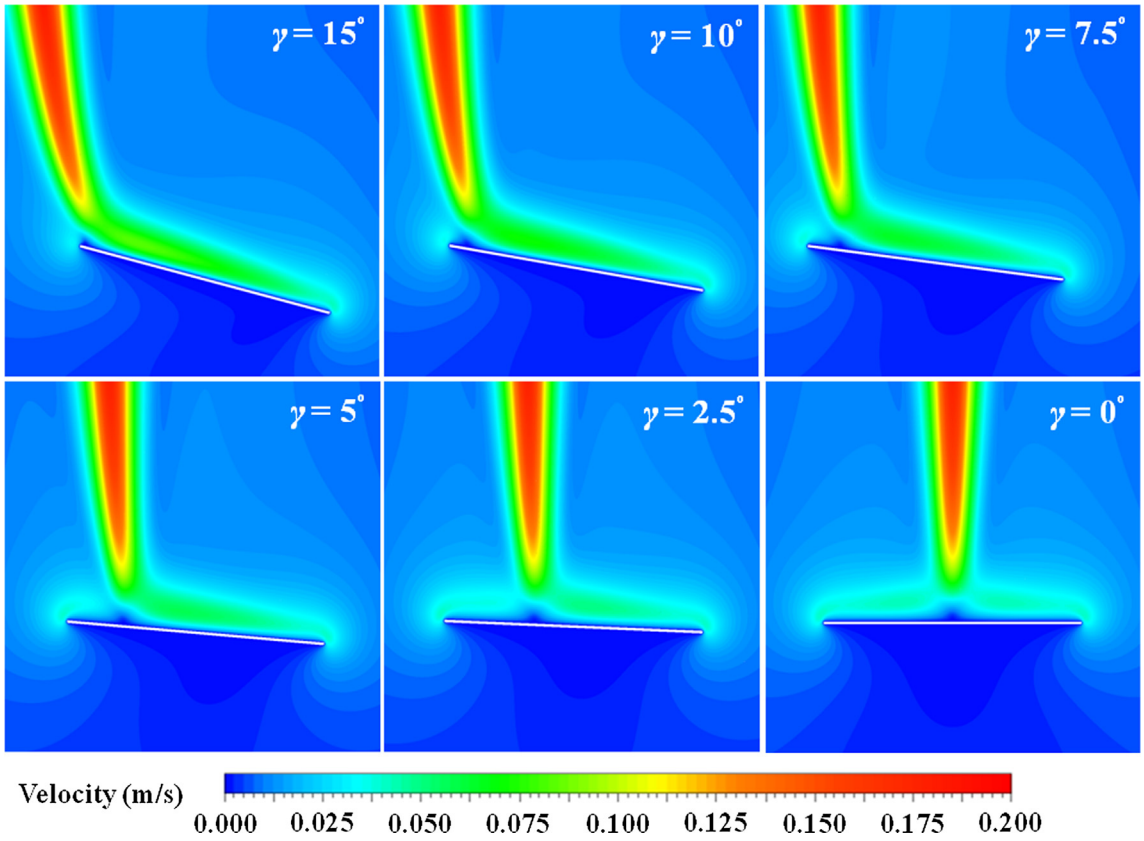

Fig. 5. Velocity contours adjacent to isothermally heated inclined plates at various inclinations of the plate in the range $0^\circ \leqslant \gamma \leqslant 15^\circ$. (Predictions of the present CFD simulations for Pr = 0.7 and $Gr_L = 10^6$ with $T_w - T_\infty = 25$ K.)

Finally, although the stagnation region formed on the insulated side was also observed for $\gamma > 15^\circ$, its expanse increases significantly at the lower inclinations shown in Fig. 5.

The contours of the magnitude of the overall velocity at various inclinations are shown in Figs. 4 and 5. However, velocity is a vector quantity and the aspect of direction is not represented in the above-mentioned contour diagrams. Thus the components of velocity are shown in Fig. 6 to reveal more details of the flow field, at three inclination angles: vertical, horizontal and $\gamma = 45^\circ$. The component of velocity along the x-direction (along the plate, see Fig. 1) is u. The component along the y-direction (normal to the plate, pointing away from the plate on the heated side of the plate) is the velocity component v. The origin of x and y is situated at the leading (right) edge of the heated side. It is to be noted that, with respect to any globally fixed co-ordinate system, the co-ordinate axes x and y (and hence u and v) rotate with the plate as its inclination is varied. Different ranges for the colour bars are used for the six sub-plots contained in Fig. 6 to bring out clearly the flow details. One needs to keep in mind, while comprehending the effects of plate inclination, the fact that the velocity in the plume increases as the vertical distance from the plate increases.

Fig. 6 shows that at all inclination angles, the u component dominates over the v component inside the boundary layer region. The striking fact is that the previous statement is true even in the case of $\gamma = 45^\circ$; the v component is generally two orders of magnitude lower than the u component inside the boundary layer on the heated side of the plate. However, the variation in the relative importance of the two components inside the plume is complex: u is the dominant component for the vertical plate, v is the dominant component for the horizontal plate, whereas both u and v are of importance for the case of the plate inclined at 45°. Another important point should be noted that the magnitude of the u-velocity inside the boundary layer of the vertical plate is far greater than that of the horizontal plate. The two different mechanisms - direct buoyancy and indirect pressure difference - operative in the two cases are responsible for this difference in the magnitude of the u-velocity. The existence of both positive and negative u-velocity of equal magnitude in the two halves above the horizontal plate is consistent with the growth of two boundary layers toward the centre of the plate in the two halves. The existence of both positive and negative v-velocity of nearly equal magnitude in the two sides of the plume for the vertical plate indicates nearly similar flow entrainment from the two sides into the plume.

Fig. 7 shows the temperature contours for inclination angles in the range $30^\circ \leqslant \gamma \leqslant 90^\circ$. Unlike the contours of velocity, the temperature is found to reach the ambient value relatively close to the heated plate (in all regions except in the buoyant plume) for all inclination angles shown. While it was found from the velocity contours (Fig. 4) that the maximum velocity in the plume increases as the vertical distance from the left edge increases, the maximum value of the temperature inside the buoyant plume decreases as the vertical distance above the plate increases. The temperature contours for inclination angles in the range $0^\circ \leqslant \gamma \leqslant 15^\circ$ are shown in Fig. 8. The principal differences between the contours in Figs. 7 and 8 are the change in the location where the buoyant plume lifts off from the heated plate, and the development of a second thermal boundary layer from the left edge at the small inclination angles.

Figs. 9 and 10 show the contours of gauge static pressure around the inclined plate for various inclination angles from vertical to horizontal. As in case of the velocity and temperature contours, we have shown the pressure contours in two separate groups of inclination angles: (i) $30^\circ \leqslant \gamma \leqslant 90^\circ$ in Fig. 9 and (ii) $0^\circ \leqslant \gamma \leqslant 15^\circ$ in Fig. 10. It is observed in Fig. 9 that low gauge pressure zones exist in the vicinity of the trailing edge as well as the

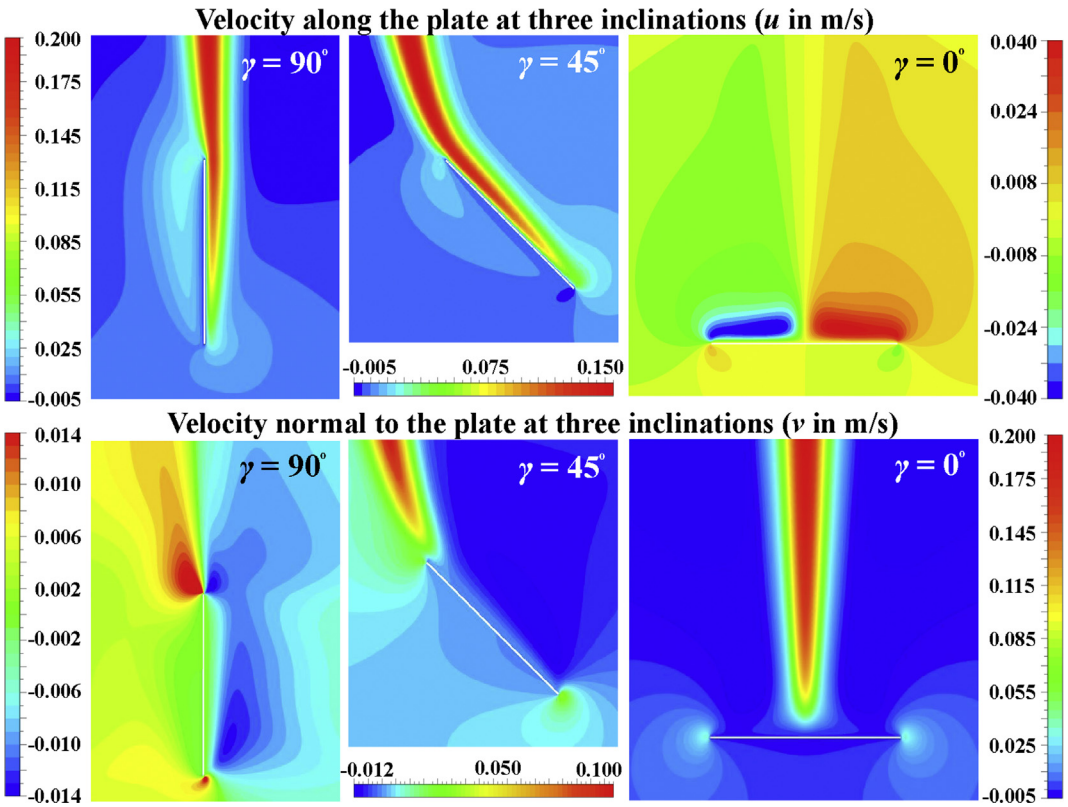

Fig. 6. Contours of velocity components along and normal to the isothermally heated plate for three inclination angles. (Predictions of the present CFD simulations for Pr = 0.7 and $Gr_L = 10^6$ with $T_w - T_\infty = 25$ K.)

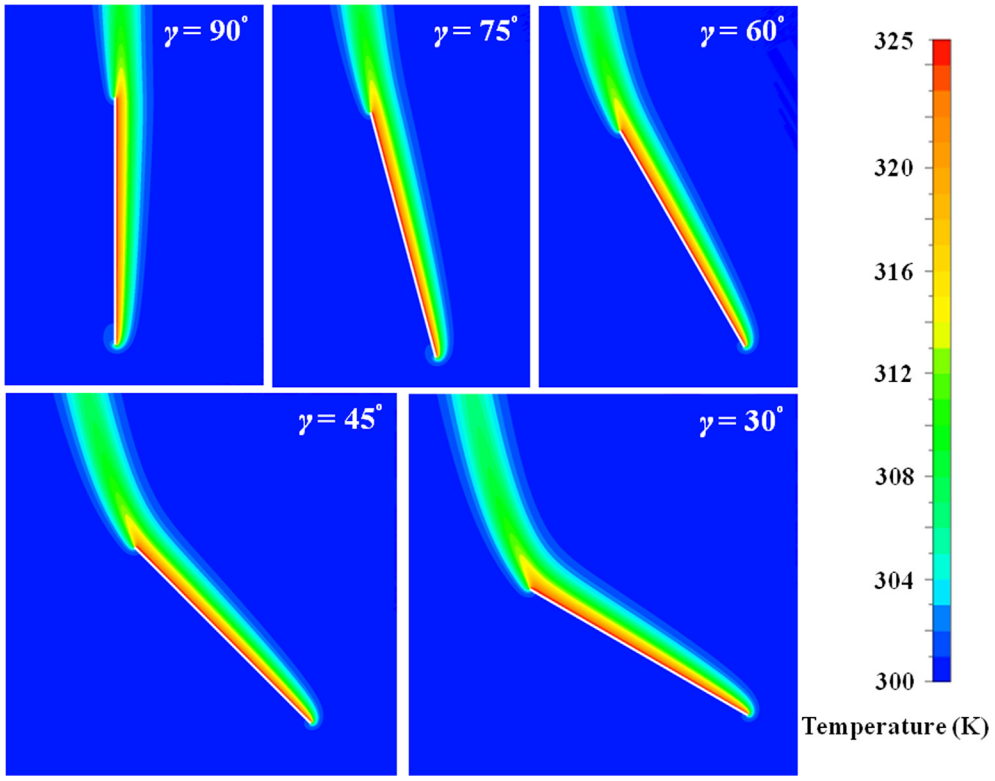

Fig. 7. Temperature contours adjacent to isothermally heated inclined plates at various inclinations of the plate in the range $30^\circ \leqslant \gamma \leqslant 90^\circ$. (Predictions of the present CFD simulations for Pr = 0.7 and $Gr_L = 10^6$ with $T_w - T_\infty = 25$ K.)

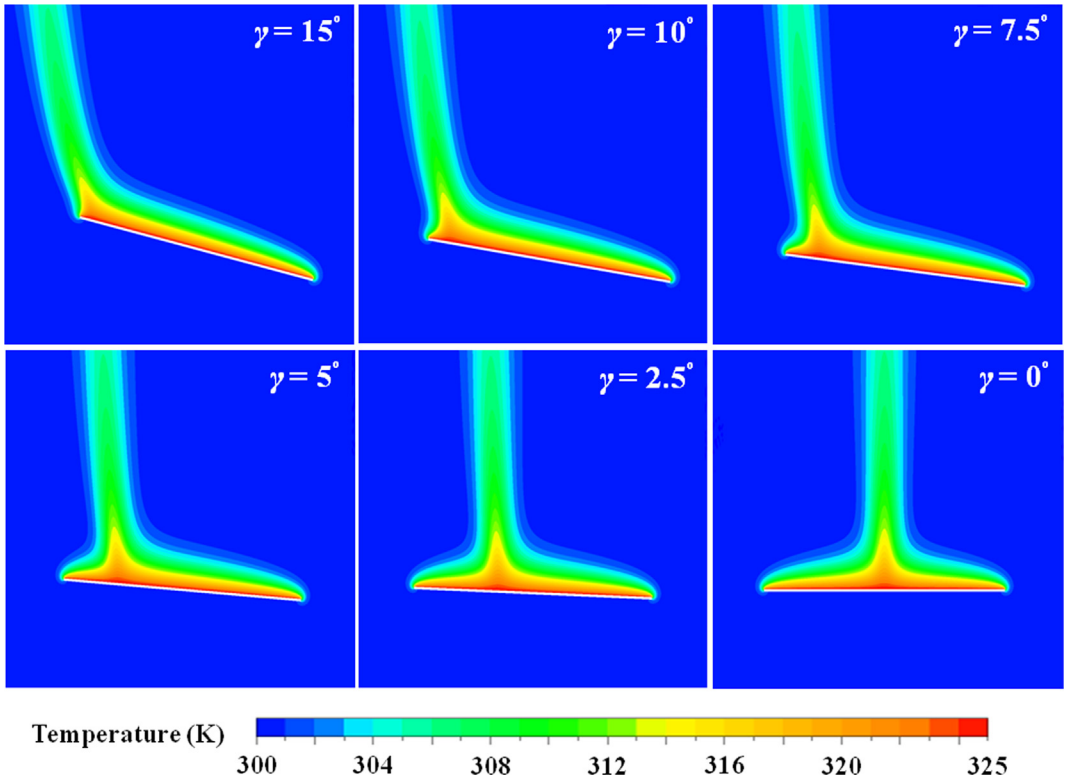

Fig. 8. Temperature contours adjacent to isothermally heated inclined plates at various inclinations of the plate in the range $0^\circ \leqslant \gamma \leqslant 15^\circ$. (Predictions of the present CFD simulations for Pr = 0.7 and $Gr_L = 10^6$ with $T_w - T_\infty = 25$ K.)

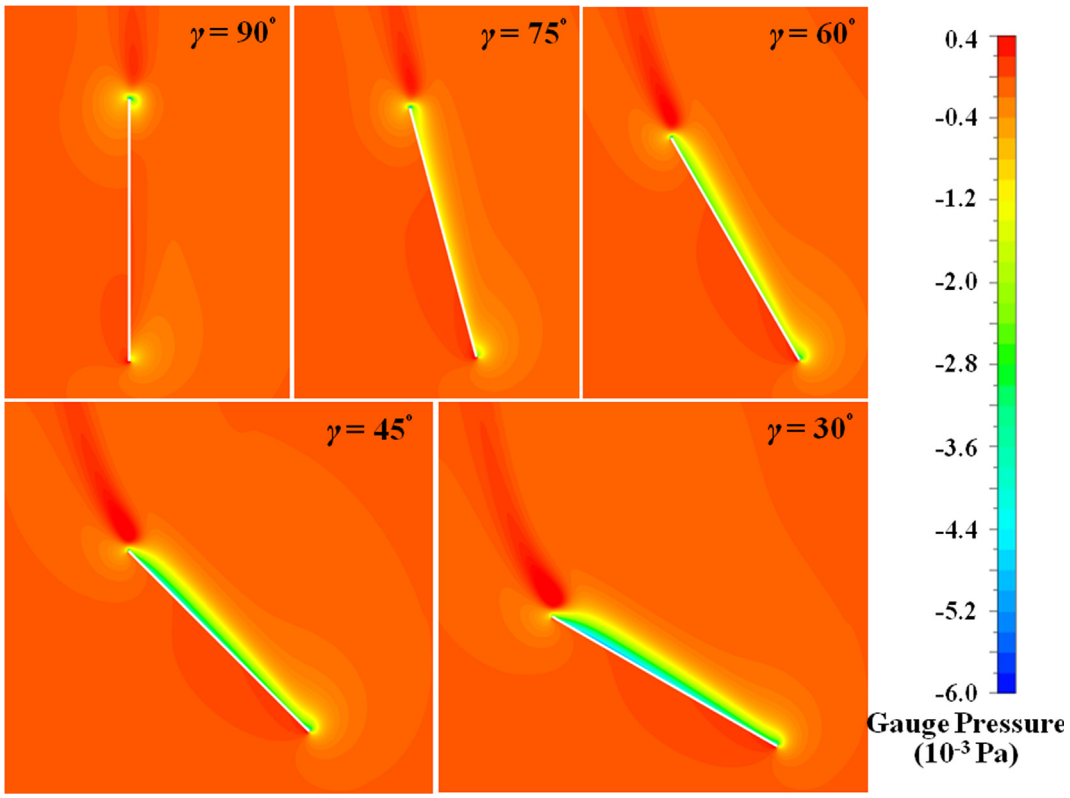

Fig. 9. Pressure contours adjacent to isothermally heated inclined plates at various inclinations of the plate in the range $30^\circ \leqslant \gamma \leqslant 90^\circ$. (Predictions of the present CFD simulations for Pr = 0.7 and $Gr_L = 10^6$ with $T_w - T_\infty = 25$ K.)

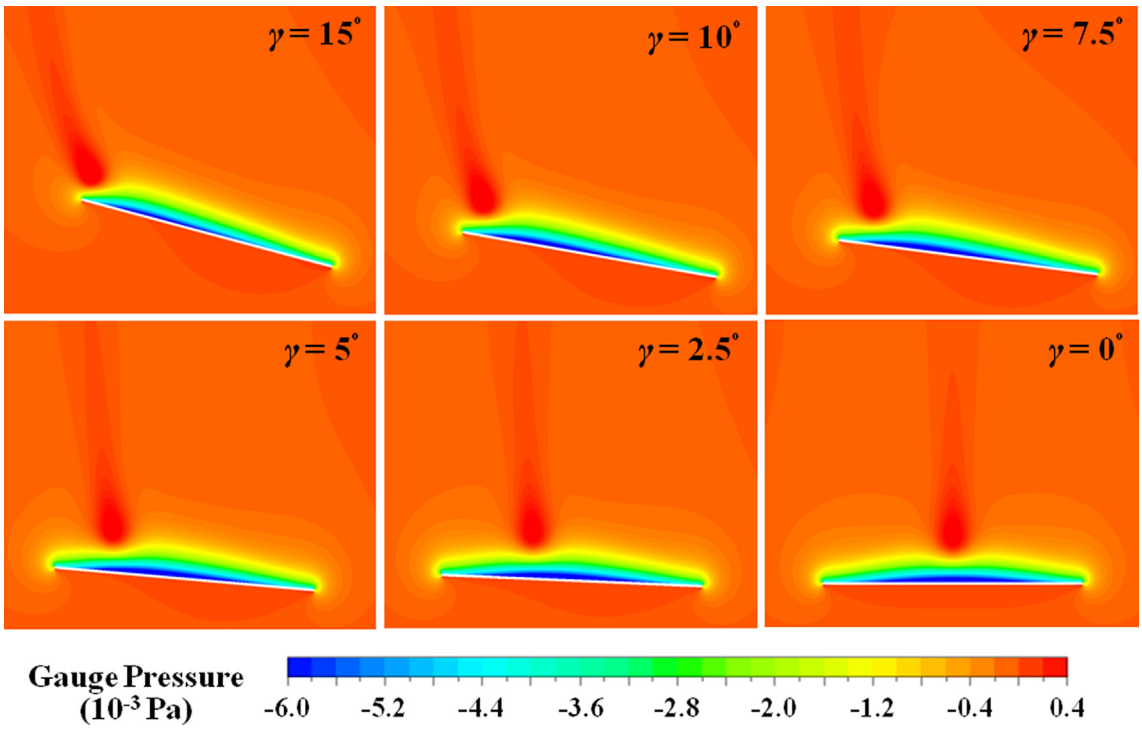

Fig. 10. Pressure contours adjacent to isothermally heated inclined plates at various inclinations of the plate in the range $0^\circ \leqslant \gamma \leqslant 15^\circ$. (Predictions of the present CFD simulations for Pr = 0.7 and $Gr_L = 10^6$ with $T_w - T_\infty = 25$ K.)

leading edge on the heated side of the plate. For the vertical orientation the gauge pressure (close to the surface) in the central part of the heated surface is slightly positive, but for other angles a region of relatively low negative gauge pressure develops there, and the expanse of this region (perpendicular to the plate) increases as the inclination angle decreases. The pressure contours of Fig. 9 show that, although the level of low pressure in the central region depends on the inclination angle, there is no appreciable change in its magnitude along the plate for any particular inclination angle. This shows that the flow inside the boundary layer in the range $30^\circ \leqslant \gamma \leqslant 90^\circ$ is not primarily caused by indirect pressure difference but arises by the direct effect of buoyancy. Fig. 9 further shows that the buoyant plume is characterized by a relatively high gauge pressure whose magnitude decreases as the vertical distance along the plume increases. The greater pressure in the central region of the plume may be attributed to the meeting of the two entrained fluid streams from the two sides of the plume. Fig. 9 also shows the development of a region of positive gauge pressure on the insulated (left) side of the plate, particularly close to the leading edge. Thus, there exists a pressure differential across the inclined plate with a low gauge pressure region on the heated surface and a relatively high gauge pressure region on the insulated surface opposite to it.

The contours of pressure around the inclined plate for $0^\circ \leqslant \gamma \leqslant 15^\circ$ are shown in Fig. 10. Like Fig. 9, the pressure contours in Fig. 10 are also characterized by the existence of a pressure differential across the plate (with lower pressure on the heated side) and positive gauge pressure inside the buoyant plume. However, it is found that for the small inclination angles, there exists a gradient of gauge pressure parallel to the plate (indicated by the shape of the contour bands near the plate). The location of minimum gauge pressure (on the heated side) shifts toward the centre of the plate as γ approaches 0°. It is also seen in Fig. 10 that, on the insulated side of the plate, the region of relatively high gauge pressure is present principally in the first half of the plate ($x < L/2$) starting from the right edge at $\gamma = 15^\circ$, but it occupies the full extent from the right edge to the left edge as $\gamma \to 0^\circ$.

Fig. 11 shows a number of important differences between the natural convection mechanisms for horizontal and vertical plates. The region of lowest static pressure occurs around the centre of a horizontal surface (Fig. 11a), whereas that occurs near the leading and trailing edges of a vertical plate (Fig. 11b). Several contour lines of static pressure meet the horizontal surface, indicating that there is a pressure gradient along the horizontal surface that is primarily responsible for fluid flow in the natural convective boundary layer above a heated horizontal plate. The pressure gradient acts from the two edges of the horizontal plate towards the centre of the plate. The gauge static pressure is nearly constant in a region of large vertical extent close to the isothermally heated surface (right hand side) of the vertical plate, indicating that there is negligible pressure gradient along the surface and this makes negligible contribution to the fluid flow in the natural convective boundary layer close to a heated vertical plate (here the fluid motion takes place because of the direct buoyancy force). The small changes in gauge static pressure around the leading and trailing edges of a vertical plate are due to the effects of finiteness of the plate. Another important difference lies in the magnitude of the static pressure difference. Fig. 11 shows that the static pressure difference for a horizontal plate is an order of magnitude greater than that for a vertical plate. On the other hand, a study of Figs. 4 and 5 reveals that the magnitude of the velocity along the plate (u) within the boundary layer is about an order of magnitude greater for the vertical plate as compared to that for the horizontal plate. The magnitude of velocity, however, reaches similar order in the plume for both cases (being only slightly lower in the case of horizontal plate).

Our aim is to present a clear exposition of the details of the flow physics which occur at different scales. We have selected various extents of the flow domain or the scales of axes in the figures given in this paper - these choices are not arbitrary, but are based on

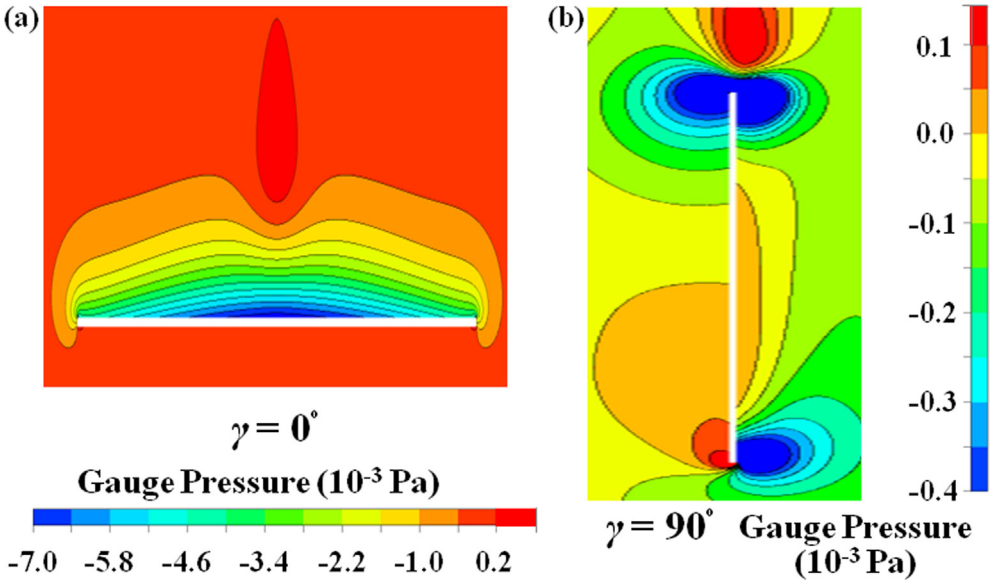

Fig. 11. Magnified pressure contours adjacent to isothermally heated plates. (a) horizontal plate ($\gamma = 0^\circ$), (b) vertical plate ($\gamma = 90^\circ$). (Predictions of the present CFD simulations for Pr = 0.7 and $Gr_L = 10^6$ with $T_w - T_\infty = 25$ K. The axis perpendicular to the plate is greatly stretched to clarify the details of the pressure variation within the boundary layer close to the plate.)

painstaking experimentation with these parameters. We have finally adopted the figures that, we believe, explain the physics best. For example, in Fig. 3 we have shown the flow solution in the entire computational domain. While this figure shows the quality of computational implementation in terms of the requirement for natural convection that the flow variables should approach quiescent values asymptotically, this domain for the figure cannot reveal the fine details close to the solid surface or those in the thermal plume. Hence it was necessary to select another domain of interest for displaying the contours in Figs. 4–10. Yet another domain needed to be selected for Fig. 11, because we wanted to computationally demonstrate, for the first time, the "induced" or "indirect pressure difference" whose principle has been qualitatively mentioned previously but nobody has previously demonstrated it quantitatively. To this effect, we had to significantly stretch the axis perpendicular to the plate, otherwise a clear quantitative demonstration would not be possible. Thus the differences in the sizes of the selected domains in various figures are carefully designed.

4.2. The nature of the buoyant plume

4.2.1. Consequence of the finiteness of the plate: Existence of a plume

The similarity theory, integral theories and other integro-differential formulations for natural convection assume that the plate is semi-infinite in the direction of growth of the convective boundary layer. All practical plates are, however, necessarily finite in size. It is interesting to note that the nature of CFD solutions is also such that a finite size must be specified, for which the computational domain needs to be selected and an appropriate grid needs to be constructed. The effects of this finiteness have been analysed in two recent CFD studies of natural convection around a heated horizontal plate [1] and that around a heated vertical plate [2]. The present study extends this analysis to plates at arbitrary inclination.

A direct consequence of the finiteness of the size of the plate is that the growth of the natural convective boundary layer does not continue indefinitely but results into a buoyant plume. When the heated plate is vertically oriented, upward, buoyancy-driven flow takes place along the plate and the plume forms at the trailing edge of the vertical plate. On the other hand, the flow conditions above a heated finite plate, when it is placed horizontally, are identical at the two ends of the plate. So natural convective boundary layers form at both ends, and these grow toward the centre of the plate. As the two boundary layers meet, at the centre, a plume forms. Thus the plume forms at the centre of the top surface of heated horizontal plate. The question then is how the transition of the position of the plume takes place as the inclination of the plate is progressively altered from the vertical to the horizontal.

4.2.2. The nature of the plume when the plate is vertical ($\gamma = 90^\circ$)

The thermo-fluid-dynamics of the plume and its space-wise evolution is comprehensively described in Ref. [2]. Figs. 4 and 7 show respectively the velocity and temperature contours obtained by the present CFD simulations for $\gamma = 90^\circ$. The right side of the plate is at a raised but uniform temperature (isothermally heated). The other three sides of the plate are insulated. The flow field and the temperature field on the left and right sides of the plate are not the same (left-right asymmetry). The main natural convective boundary layer forms on the right side; however, Fig. 4 shows that there is a small movement of the fluid on the left side of the plate as well, as a small fraction of the entrained fluid at the leading edge of the plate spills over to the left side. As the buoyant plume leaves the trailing edge of the plate, it bends over the plate (see $\gamma = 90^\circ$ in Fig. 4) due to the left-right asymmetry and due to the finite thickness of the plate.

As the plume leaves the plate, more and more fluid can be entrained from the left side as well. Consequently, as the vertical distance above the plate (denoted here by Y) increases there is a tendency for the centreline of the plume to align with the mid-plane of the plate, and, for the velocity of entrainment at the left and that at the right to equilibrate.

From the temperature contour for $\gamma = 90^\circ$ in Fig. 7, it can be seen that the maximum temperature of the fluid occurs close to the plate. The maximum value of temperature inside the free plume occurs around the centreline of the plume but its magnitude decreases as the vertical distance above the plate increases. The velocity along the centreline of the buoyant plume, in contrast, tends to increase as the vertical distance increases (see Fig. 4), as a consequence of buoyancy and the continued entrainment of

surrounding fluid. The asymmetry of the buoyant plume could be visualized from the contour plots in Figs. 4 and 7. The asymmetry arises for two reasons: (i) different boundary conditions being applied on the two sides of the plate, and, (ii) a finite thickness being assigned to the plate. The asymmetry is reflected in the profiles of u-velocity (representing the vertical velocity in the plume), v-velocity (which determines the mass flow rate of entrainment from the two sides of the plume) and the static temperature.

The physics of the evolution of the asymmetry was studied for the first time in Ref. [2]; a summary of the qualitative and quantitative findings is given below for ready reference.

(i) At $Y/L = 0$, i.e. even at a horizontal plane flush with the trailing edge of the plate, there exists a distribution of vertical velocity on the left (insulated) side of the plate. This is consistent with our earlier description that there exists a small natural convective current on the insulated side of the plate. (ii) As Y/L increases, i.e. as the plume moves further above the plate, there is a tendency to restore left-right symmetry in the u-velocity distribution. This happens mainly through adjustment in the velocity distribution on the left side; the velocity distribution on the right side changes only a little. (iii) The maximum value of the u-velocity increases with increasing Y/L. (iv) The previous two behaviours occur over different length scales. The restoration of the left-right symmetry happens rather quickly; the plume becomes reasonably symmetric (the right side, though, still having slightly greater velocity) when $Y/L \sim 1$. The maximum u-velocity, on the other hand, is seen to increase considerably even as far as $Y/L \sim 4$. (v) At $Y/L = 0$, there are two maxima in the u-velocity distribution, one on the left and the other on the right side. At $Y/L = 0.1$, the profile has the only maxima on the right. The transition from two-maxima to one-maxima solution is interesting and is virtually accomplished by $Y/L \sim 0.05$. (vi) As Y/L increases, the location of the maximum u-velocity shifts toward the left, tending toward the vertical line drawn through the middle of the plate. (vii) The equilibration of temperature profile takes place in the following manner as Y/L increases. At $Y/L = 0$, the temperature profile is most asymmetric with a step change at $y = 0$. As Y/L increases, the location of the maxima in temperature moves at first to the right (i.e. toward the heated side of the plate) and then to the left. Like the profile of streamwise velocity, the temperature profile also becomes nearly symmetric at $Y/L \sim 1$, though the plume still remains buoyant, and, the evolution of temperature and axial velocity continues up to much larger value of Y/L.

It is shown that at large values of Y/L, the buoyant plume tends to be symmetric with respect to an axis that seems to pass through the vertical mid-plane of the plate. An interesting interpretation of this phenomenon is that, sufficiently above the plate, the plume tends to lose its history of origination.

4.2.3. The nature of the plume when the plate is horizontal ($\gamma = 0^\circ$)

The details of the two-dimensional and three-dimensional structure of the buoyant plume are described in Ref. [1]. Here we summarize a few important points. The centreline of the plume is the plane of symmetry, i.e. the vertical line drawn at the middle of the horizontal plate. At any distance above the plate, there is left-right symmetry in the profiles of the velocity and temperature. The magnitude of velocity inside the plume is large as compared to the other regions of the domain. It can be shown that the direction of velocity within the plume is almost normal to the hot surface; and v is the major component. The plume-width broadens slowly after a certain vertical distance from the heated surface ($\gamma = 0^\circ$ in Fig. 5). This occurs due to the horizontal diffusion which introduces a non-zero u-velocity required for the entrainment within a buoyant plume. Within the plume, the variation of temperature in the y-direction is relatively small as compared to that in the boundary layer regions (Fig. 8).

Fig. 5 also shows two wing-shaped boundary layers which are developed above the heated surface. The major component of velocity within the boundary layers is u (which is parallel to the hot surface). Near the leading edges of the plate (i.e. at $x = 0$ and $x = L$), the velocity boundary layers are distorted due to the edge effect. In case of thermal boundary layers (see $\gamma = 0^\circ$ in Fig. 8), such distortion near the edges is comparatively small. From the leading edges towards the plume, the thickness of boundary layers increases. In the y-direction within the boundary layers, with increasing distance from the heated surface, the temperature decreases (Fig. 8); whereas, velocity first increases to attain a maximum value and then onward decreases (Fig. 5).

Another region shown in Fig. 5 is the junction between boundary layer regions and the plume. To describe an axisymmetric plume above a planar boundary, Whittaker and Lister [45] called the junction as 'turn-round region'. According to them, the flow within boundary layers feeds the plume through the turn-round region; and, in the turn-round region, the effect of advection predominates over the effect of diffusion. Fluid streams, from two opposite ends of the plate, move towards the plane of symmetry. However, prior to vis-à-vis collision, flow separation takes place. It is already mentioned that within the boundary layers, the major component of velocity is u, whereas within the plume, the major component of velocity is v.

4.2.4. The nature of the plume when the plate is at arbitrary inclination

Figs. 4–10 show the contours of velocity, temperature and pressure as the inclination angle γ is varied from 90° (vertical) to 0° (horizontal). The following observations may be made. (i) At $\gamma = 0^\circ$, the plume axis is vertical. At all other angles, the plume eventually tries to rise vertically, i.e. tends to align itself with the line of action of gravity. The plume thus tends to lose its history of origination. (ii) At $\gamma = 0^\circ$, there is left-right symmetry in the profiles of the velocity and temperature, at any distance above the plate. At all other values of γ, the profiles of velocity and temperature are asymmetric at the base of the plume, but the profiles evolve to become more and more symmetric as one moves upward along the plume. The details of the equilibration process for the vertical plate are given in Section 4.2.2. (iii) The predominant direction of motion inside the plume is upward along the centreline of the plume. For the horizontal plate, the flow in the boundary layer is predominantly parallel to the plate surface and toward the centre (moving in from two ends of the plate); when these fluid streams approach each other near the centre of the plate, they combine to move the fluid in the perpendicular direction which is the predominant direction of fluid motion inside the plume. For the vertical plate, the predominant direction of motion in the boundary layer is also upward, and this upward motion is enhanced in the buoyant plume because of entrainment. The two streams of entrained fluid from the left and right converge towards each other, with the consequent change of direction by 90°. At intermediate values of γ, both horizontal and vertical mechanisms are operative. (iv) The value of maximum temperature at a cross-section of the plume decreases as one moves away from the plate; this tendency is opposite to that in the variation of the maximum velocity in the plume which increases with distance from the plate.

In order to obtain a quantitative summary of the spatial evolution of the plume for an inclined heated plate, we define two new axes X and Y with the origin situated at the trailing (left) edge on the heated surface. The axis X represents the horizontal and the axis Y represents the vertical direction. X is positive rightward and Y is positive upward (gravity acts in the negative Y direction). The directions of X and Y remain invariant with any value of inclination angle γ. Fig. 12 shows the inter-relations of the new axes $X - Y$ and the axes $x - y$ that were introduced in Fig. 1. It is recalled

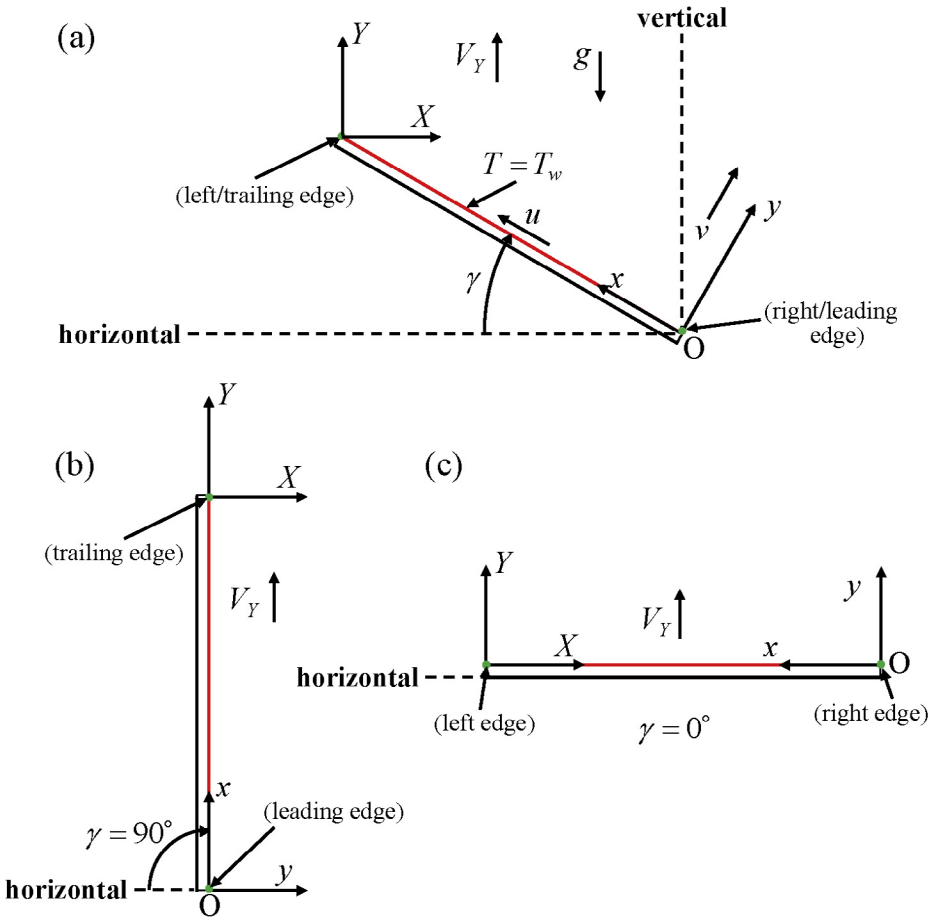

Fig. 12. Inter-relationship of two co-ordinate systems $X - Y$ and $x - y$. (a) Plate at a general inclination angle γ, (b) plate is vertical ($\gamma = 90°$), (c) plate is horizontal ($\gamma = 0°$).

that the co-ordinate x is along the plate, y is perpendicular to the plate and, the origin lies at the leading (or right) edge of the heated side of the plate. Through trigonometric manipulations, the new co-ordinates X and Y may be related to the co-ordinates x and y, by the following relations: $X = (L - x)\cos\gamma + y\sin\gamma$ and $Y = (x - L)\sin\gamma + y\cos\gamma$, where L is the length of the plate. For a vertical plate $\gamma = 90°$, and therefore, $X = y$, $Y = x - L$ (Fig. 12b). For a horizontal plate $\gamma = 0°$, and therefore, $X = L - x$, $Y = y$ (Fig. 12c).

The component of velocity along the $Y-$ axis is denoted by V_Y. Through simple trigonometry it may be established that $V_Y = u\sin\gamma + v\cos\gamma$, where u is the velocity parallel to the heated plate and v is the velocity perpendicular to the plate. V_Y is used in this work as the characteristic velocity in the plume for a generalized description of the plume. Since the plume centreline bends as the plume rises, and the bending depends on the inclination angle γ, we felt that the best universal choice for the characteristic velocity in the plume, that would remain invariant irrespective of changing values of γ, is V_Y. This is supported by the physical feature that eventually all plumes, for whatever value of γ, tends to align with the $Y-$ axis. The adopted definition of V_Y behaves appropriately in the two limits. When $\gamma = 90°$, $V_Y = u$: this makes physical sense since the velocity along a vertical plate is in the same direction as the predominant velocity in the plume. When $\gamma = 0°$, $V_Y = v$: this also makes physical sense since the predominant velocity in the plume is normal to a horizontal plate.

As a quantitative example of the spatial evolution of the plume for an inclined plate, the profiles of characteristic velocity V_Y and static temperature T for $\gamma = 75°$ are shown respectively in Figs. 13 and 14. The co-ordinate axes X and Y are shown inside Figs. 13 and 14 for clarity. Certain features of the spatial evolution of V_Y and T for inclined plates remain broadly similar as was discussed in the case of vertical plate (Section 4.2.2). For example, as Y/L increases: (i) profiles of both V_Y and T tend to be more symmetric about a vertical line, (ii) the maximum value in the profile of V_Y increases

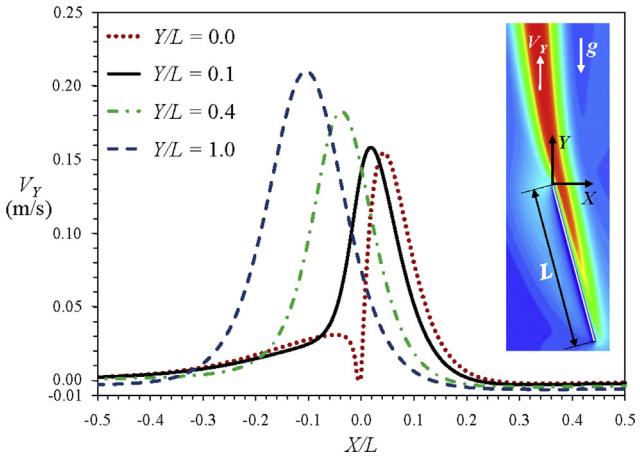

Fig. 13. Progressive development of the vertical velocity V_Y profile in the buoyant plume at different heights above the top edge of an inclined plate. (Predictions of the present CFD simulations for $\gamma = 75°$, Pr = 0.7 and $Gr_L = 10^6$. As Y/L increases, the profile becomes progressively more symmetric, the maximum increases and the location of the maximum shifts to the left. Note that new axes X and Y are defined for the study of spatial evolution of the plume.)

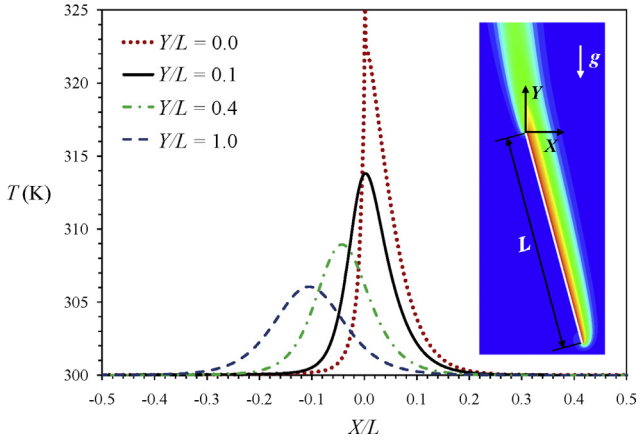

Fig. 14. Progressive development of the temperature profile in the buoyant plume at different heights above the top edge of an inclined plate. (Predictions of the present CFD simulations for $\gamma = 75^\circ$, Pr = 0.7 and $Gr_L = 10^6$ with $T_w = 325$ K. As Y/L increases, the profile becomes progressively more symmetric, the maximum decreases and the location of the maximum shifts to the left. Note that new axes X and Y are defined for the study of spatial evolution of the plume.)

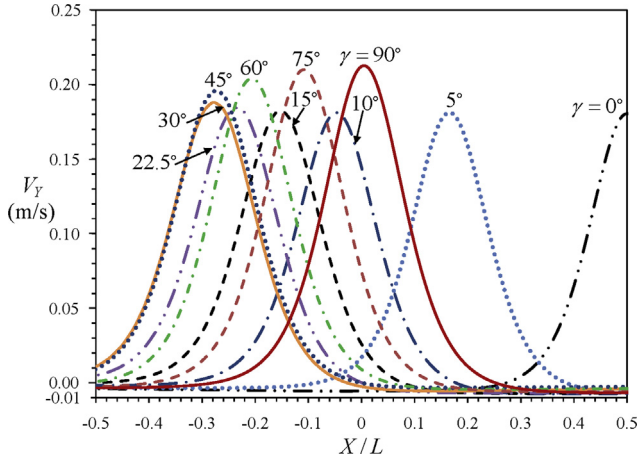

Fig. 15. Variation of the vertical velocity V_Y profile in the buoyant plume at a particular height ($Y/L = 1$) above the top edge of an inclined plate with changing values of inclination angle γ. (Predictions of the present CFD simulations for Pr = 0.7 and $Gr_L = 10^6$. Note that new axes X and Y are defined for the study of spatial evolution of the plume.)

because of buoyancy and entrainment, (iii) the maximum value in the profile of T, on the other hand, decreases and tends toward T_∞ because of transport of heat.

There are, however, two mentionable differences between the nature of the plume over an inclined plate and that over a vertical plate: one subtle and the other substantial. The subtle difference lies in the profiles of V_Y and T at $Y/L = 0$. For the vertical plate the solid edge of thickness t_P is aligned with the horizontal line $Y/L = 0$. The profile in velocity V_Y therefore contains a span t_P at zero velocity because of the no penetration boundary condition. Similarly, the profile in static temperature T contains a span t_P representing the temperature of the adiabatic solid edge. For the inclined plate, however, only the corner point at the trailing (left) edge forms part of the line $Y/L = 0$, all other points of the solid edge lie below the line $Y/L = 0$. All points of the profiles in V_Y and T, except the origin of the axes X, Y therefore represent the velocity and temperature in the interior of the fluid.

Now we discuss the substantial difference between the nature of the plume over an inclined plate and that over a vertical plate. The locations of the maxima in both V_Y and T profiles shift as Y/L changes; the extents of the loci of the two maxima were shown to be finite but quite small for the vertical plate [2]. The corresponding extents in the excursion of maxima for inclined plates can, however, be large. Since the predominant direction of motion in the convective boundary layer is along the plate surface, as the plate is tilted further from the vertical there remains a greater component of this convective velocity in the negative X direction. This pushes the maxima in the V_Y and T profiles toward the left of the trailing (left) edge. In order to obtain a quantitative understanding of this behaviour as a function of the inclination angle γ, the profiles of V_Y at a fixed value of Y/L are constructed for various values of γ. The results for $Y/L = 1$ are shown in Fig. 15. It is found that, in line with the physical explanation just given, the maximum value decreases and its location shifts toward the left (i.e. occurs at greater value of negative X/L) as the inclination angle decreases. This trend, however, must reverse at a certain value of γ, because we know from the discussion in Section 4.2.3 for the horizontal plate that the maximum occurs above the middle of the plate (i.e. at $X/L = 0.5$), which is situated to the right side of the corner of the trailing (left) edge. When the full data like what is shown in Fig. 15 are analysed, it is found that the reversal happens at a value of inclination angle such that $\gamma_{reversal} \sim 30^\circ$ (for the chosen Y location, $Y/L = 1$). As γ is progressively decreased below $\gamma_{reversal}$ up to $\gamma = 0^\circ$, the value of maximum V_Y decreases slightly and the location of the maximum moves to the right. This rightward movement of the location of the maximum is a strong function of γ. Fig. 15 shows that the location of the maximum is at $X/L = -0.15$ for $\gamma = 15^\circ$ and at $X/L = +0.5$ for $\gamma = 0^\circ$.

4.3. The lift-off point: definition, quantification and significance

Figs. 4–10 show that the location of the rise of plume from the plate shifts from the trailing edge of the plate for $\gamma = 90^\circ$ (vertical plate) to the centre of the plate for $\gamma = 0^\circ$ (horizontal plate). The figures visually demonstrate that almost the entire transition of this important character in the origination of the plume takes place over a rather small range of inclination angle, viz. $0^\circ \leqslant \gamma \leqslant 15^\circ$. To perform a quantitative analysis, the location of the formation of the plume needs to be pinpointed, which is achieved here by defining the lift-off point. It is believed that this is the first qualitative and quantitative study of the behaviour of the lift-off point.

Fig. 16 shows a qualitative sketch of the structure of the confluence of convective boundary layers and the evolution of the plume

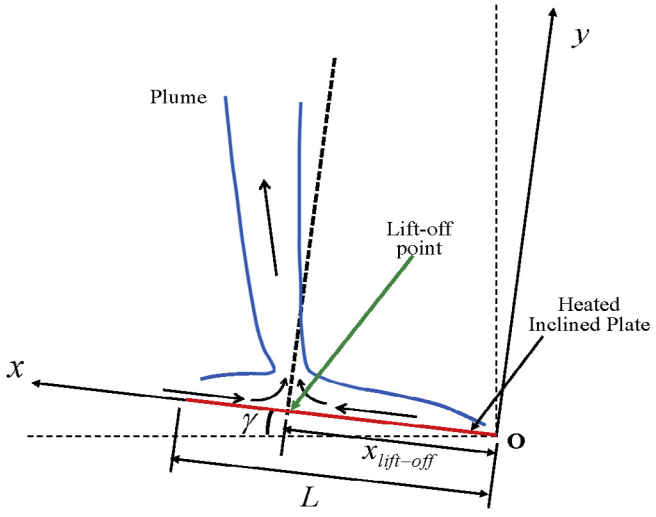

Fig. 16. A schematic diagram representing the lift-off point at small angles of inclination.

for an arbitrary inclination of the heated plate. We explained previously how the plume forms as two opposite streams moving predominantly parallel to the solid surface transform, at the point of confluence, into a stream moving at right angle to the original streams. In Fig. 17, we have plotted the ratio of (v/u) for $\gamma = 5^\circ$, since this ratio gives the orientation of the overall velocity vector relative to the plate. This ratio is plotted at three grid lines which run parallel to the plate and are close to the plate. It is found that all three curves make a sharp transition at a particular value of x, which we define as the lift-off distance from the leading (right) edge of the plate. Table 3 gives the values of non-dimensional lift-off distance $\bar{x}_{lift-off}$ at various values of inclination angle γ. It is found that $\bar{x}_{lift-off}$ is a strong function of γ in the range $0^\circ \leqslant \gamma \leqslant 15^\circ$.

The physical mechanism of natural convection on a vertical surface is very different from that over a horizontal surface. For a vertical surface, buoyancy is generated because of the temperature difference between the surface and the fluid. The buoyancy force is parallel to the surface and creates fluid motion along the vertical surface; the fluid motion carries away heat from the surface (when the surface is hotter than the surrounding fluid) or supplies heat to the surface (when the surface is colder than the surrounding fluid). On a horizontal surface, the buoyancy force is perpendicular to the surface. The natural convective motion along the horizontal surface is set up by an indirectly generated pressure difference. This pressure difference has been quantified in the computations of the present work, numerical visualizations being shown in Figs. 10 and 11.

The governing equation derived in the paper by Guha and Pradhan (Eq. (18) in Ref. [4]) beautifully captures this stark difference in the mechanisms of natural convection. For a vertical surface (i.e. $\gamma = 90^\circ$), the Term II in Eq. (18) of Ref. [4], representing the indirect pressure difference, drops out and the sole cause for the generation of natural convection on a vertical surface becomes the Term III, i.e. the direct buoyancy force. For a horizontal surface (i.e. $\gamma = 0^\circ$), on the other hand, the Term III in the same equation, representing the direct buoyancy force, drops out and the sole cause for the generation of natural convection on a horizontal surface becomes the Term II, i.e. the indirect pressure difference. For surfaces at intermediate angles, both source terms (i.e. Term II and Term III) are operative, but through a comprehensive analysis the authors were able to establish the generic trend in the relative magnitudes of the two source terms as a function of Grashof number, Prandtl number and inclination angle. These calculations are repeated here for the specific combination of parameters $Gr_L = 10^6$, $\mathrm{Pr} = 0.7$, and the variations of the relative force components are plotted as a function of the inclination angle in Fig. 18. The value of the special inclination angle $\gamma_{cross-over}$ at which buoyancy and force due to indirect pressure difference become equal decreases with increasing Grashof number, and, for $\mathrm{Pr} \geqslant 0.7$, is within 10° in the range $10^3 \leqslant Gr \leqslant 10^7$. At $Gr_L = 10^6$, $\mathrm{Pr} = 0.7$, the cross-over point is numerically determined to be at $\gamma_{cross-over} = 5.86^\circ$.

In order to explore the mechanisms of natural convection for an inclined plate, the computed values of the Nusselt number Nu_x were compared with a particular scaling of the result for vertical plate in Ref. [4]. This study revealed that, at $Gr_L = 10^6$ and $\mathrm{Pr} = 0.7$, Nu_x is almost identical with the value of $Nu_{x,vertical}(\sin\gamma)^{1/4}$ up to $\gamma \sim 15^\circ$, and significant departures from the scaling were observed only in the region $15^\circ \gtrapprox \gamma \geqslant 0^\circ$ (The departure is about 1% at $\gamma = 17^\circ$, whereas it is 41% at $\gamma = 1^\circ$). The present computations show that the lift-off point shifts from the middle of the plate to nearly the trailing (left) edge as γ is changed from 0° to 15° ($\bar{x}_{lift-off} = 0.9816$ at $\gamma = 15^\circ$, from Table 3), and the physical picture of natural convection in the range $15^\circ < \gamma \leqslant 90^\circ$ - revealed in Figs. 4, 7 and 9 - remain essentially the same as that around a vertical plate. The coincidence of the approximate range $(15^\circ \geqslant \gamma \geqslant 0^\circ)$ mentioned in the above two studies is intriguing, at least at the first sight, because in the unified integral theory of Guha and Pradhan [4] the convective boundary layer is assumed to grow from one edge of a semi-infinite plate and there is no provision for the existence of a plume. In order to shed further light on this, magnified views of the static pressure distribution close to

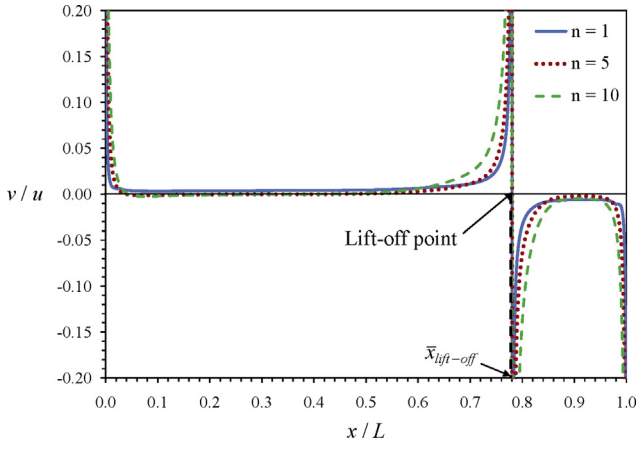

Fig. 17. Determination of the location of the lift-off point $\bar{x}_{lift-off}$ for plate inclination of 5° (at $Gr_L = 10^6$, $\mathrm{Pr} = 0.7$).

Table 3
Distance (in non-dimensional form) of lift-off point of the plume from the leading (right) edge of the plate (at $Gr_L = 10^6$, $\mathrm{Pr} = 0.7$) and the corresponding distance of the minimum heat flux point.

γ (in degree)	$\bar{x}_{lift-off} = \frac{x_{lift-off}}{L}$	$\bar{x}_{q_{x,\min}} = \frac{x_{q_{x,\min}}}{L}$
25	1	0.9668
22.5	0.9991	0.9640
20	0.9977	0.9611
17.5	0.9938	0.9550
15	0.9816	0.9466
12.5	0.9612	0.9328
10	0.9289	0.9074
7.5	0.8722	0.8572
5	0.7805	0.7709
2.5	0.6514	0.6468
0	0.5	0.5

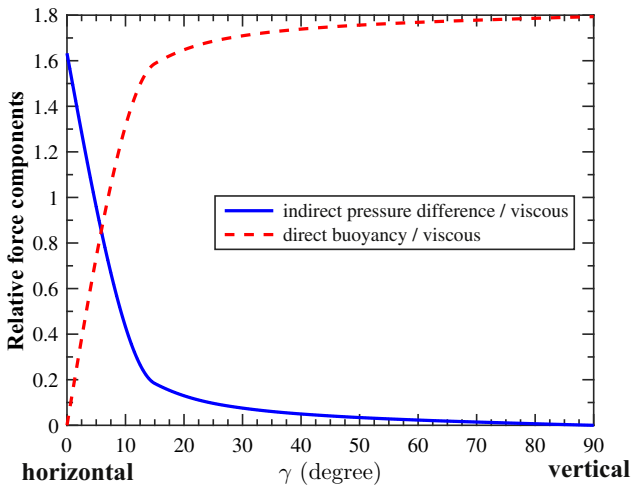

Fig. 18. Variation of the relative force components for natural convection on inclined isothermal surfaces at $Gr_L = 10^6$, $\mathrm{Pr} = 0.7$ according to the unified integral theory of Ref. [4].

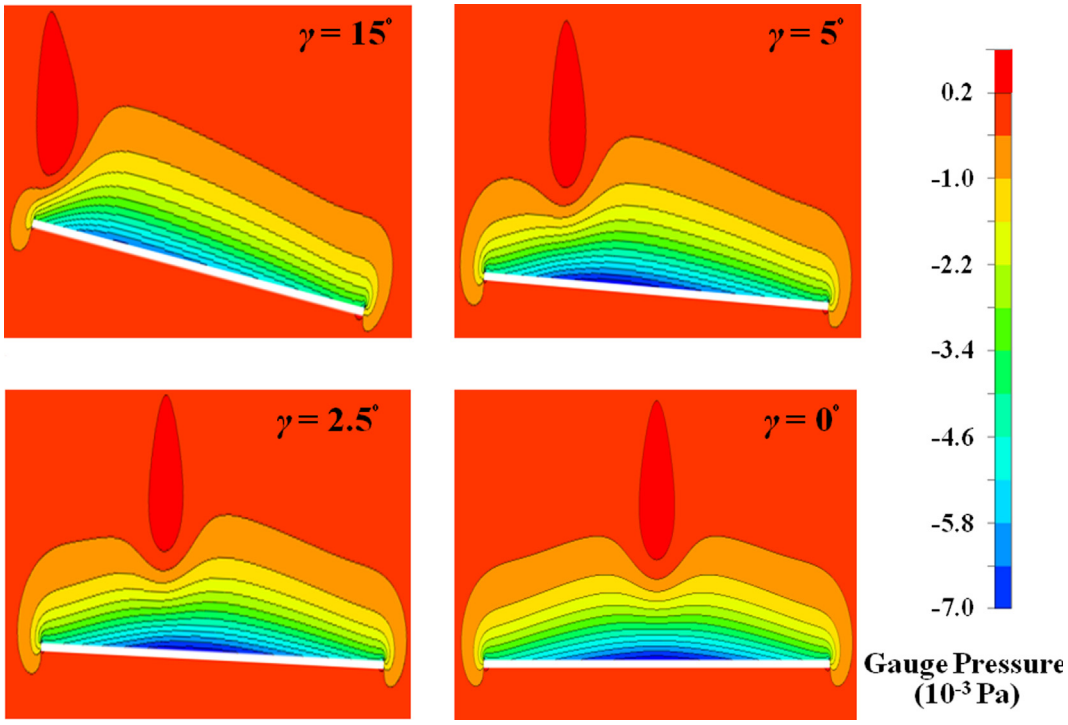

Fig. 19. Magnified pressure contours adjacent to isothermally heated plates which are horizontal or slightly inclined to the horizontal. (Predictions of the present CFD simulations for Pr = 0.7 and $Gr_L = 10^6$ with $T_w - T_\infty = 25$ K. The axis perpendicular to the plate is greatly stretched to clarify the details of the pressure variation within the boundary layer close to the plate.)

the plate in the aforementioned range of inclination angles are drawn in Fig. 19. It is found that the minimum pressure zone on the plate surface occurs approximately beneath the plume and the pressure distribution on the two sides of the lift-off point are asymmetric for all angles except for $\gamma = 0^\circ$ (when the lift-off point is in the middle of the plate and the flow in two-halves are identical). Looking at the contour lines, it is also evident that in the asymmetric flow pattern, the magnitude of the indirect pressure gradient along the surface (i.e. $\partial p/\partial x$) is greater in the region between the trailing (left) edge and the lift-off point than that between the lift-off point and the leading (right) edge. It may be further observed that, out of the four plots in Fig. 19, the extent of the lowest pressure region is the smallest at $\gamma = 15^\circ$ and the plume is almost at the trailing edge. This indicates that the magnitude of indirect pressure difference would further diminish for $\gamma > 15^\circ$. It seems that the unified integral theory, even though unaware of the presence of the plume, reasonably correctly predicts the inclination angles for which the indirect pressure difference becomes appreciable and eventually dominates over the direct buoyancy. The CFD solutions for the finite plates also capture the details of the relative magnitudes of indirect pressure difference and buoyancy as a function of the inclination angle. The CFD solutions, in addition, can capture the details of asymmetric flow from the two edges of a finite plate and the formation of the plume.

4.4. Computation of heat transfer rate

Both local and average heat transfer coefficients are computed, which lead to local and average values of the Nusselt number. Eqs. (6)-(10) show that caution is needed in the computation of the average Nusselt number $\overline{Nu}$, since the integration is performed over the heat transfer rate (and not over the local value of Nusselt number): $\overline{Nu} = \bar{h}L/k = (1/k)\int_0^L h_x dx$.

Most experimental studies mention local values of Nusselt number Nu_x, though a few also give values of $\overline{Nu}$. Gryzagoridis [13] performed experiments for natural convection from a vertical plate and reported average heat transfer rates. Rich [30] performed experiments for an aluminium plate of dimensions $40.64cm \times 10.16cm \times 0.3175cm$. Measurements were made at four points on the plate for five inclination angles, viz. 90° (vertical), 80°, 70°, 60° and 50°. The plate was tested for a range of Grashof numbers from 10^6 to 10^9. $\overline{Nu}$ was reported for the vertical case only while Nu_x was reported at all the inclination angles considered. The data for the 50° inclined plate began to show the effects of the velocity component in the third dimension, and hence lower angles were not studied as the interferometer was limited to two-dimensional problems. An aluminium alloy plate of dimensions 68.18 cm × 17.78 cm × 0.87 cm was used by Sang-Urai [31] in his investigations of natural convection from heated inclined plates. Experiments were performed for several inclination angles ranging from 90° (vertical) to 0° (horizontal), and the temperature distributions in the boundary layer were measured at several positions along the plate. The Nusselt numbers were subsequently calculated from these temperature distributions.

We have collated experimental values of Nusselt number from Refs. [13,30,31] in Table 4 in which the corresponding values obtained from the present CFD simulations are also included so that a direct comparison is possible. Many new CFD simulations, additional to what are reported in Sections 4.1–4.3, had to be run at the operating conditions of the available experimental results. The agreement between the experiments and present computations over the range of Rayleigh number and plate inclination angle is good, giving confidence in the physical conclusions made in the present study. As per our knowledge, the present work represents the most comprehensive theoretical work on natural convection above heated plates at arbitrary inclination, and Table 4 provides the most extensive experimental validation.

Table 5 shows the present results for $\overline{Nu}$ vis-à-vis the values of $\overline{Nu}$ that can be computed by integrating the results for Nu_x given in two previous theoretical studies [4,33]. Yu and Lin [33] had

Table 4
Comparison of Nusselt number obtained by present CFD simulations with experimental results.

Rayleigh number (Ra_L)	Inclination angle (γ)	Reference no. for experiment	Experimental average Nusselt number $\overline{Nu}$	Average Nusselt number from present CFD $\overline{Nu}$
7×10^5	90°	[13]	16.00	15.75
7×10^6	90°	[30]	28.00	27.28
Rayleigh number (Ra_x)			Experimental local Nusselt number (Nu_x)	Local Nusselt number from Present CFD (Nu_x)
6×10^4	90°	[31]	6.04	6.07
5×10^5	90°	[31]	10.22	10.31
3×10^6	90°	[30]	17.06	17.54
6×10^4	75°	[31]	5.77	5.95
5×10^5	75°	[31]	9.92	9.99
3×10^6	70°	[30]	16.79	17.27
6×10^4	60°	[31]	5.72	5.85
5×10^5	60°	[31]	9.62	9.69
3×10^6	60°	[30]	16.46	16.92
6×10^4	45°	[31]	5.46	5.60
5×10^5	45°	[31]	9.00	9.14
6×10^4	30°	[31]	4.95	5.14
5×10^5	30°	[31]	8.00	8.19
6×10^4	15°	[31]	4.27	4.53

Table 5
Comparison of Nusselt number obtained by present CFD simulations, numerical analysis and integral analysis for $Gr_L = 10^6$ and Pr = 0.7.

γ (in degree)	$\overline{Nu}$ (for semi-infinite plate -numerical solution) [33]	$\overline{Nu}$ (for semi-infinite plate - integral analysis) [4]	$\overline{Nu}$ (for finite plate - CFD, present study)
0	9.2685	9.6573	12.4953
2.5	9.7210	9.9830	12.4610
5	10.2099	10.4284	12.4237
7.5	10.6315	10.8451	12.3759
10	11.0013	11.2317	12.3858
12.5	11.3310	11.5890	12.4963
15	11.6286	11.9189	12.6704
17.5	11.9460	12.2239	12.8774
20	12.1958	12.5062	13.0883
22.5	12.4261	12.7681	13.2951
25	12.6391	13.0119	13.5117
30	12.9686	13.4483	13.8999
45	13.8256	14.4420	14.8284
60	14.3612	15.0691	15.4232
75	14.6456	15.4014	15.7248
90	14.875	15.5714	15.7503

numerically solved, by finite-difference method, the boundary layer equations for natural convection around a semi-infinite heated inclined plate, using a complex co-ordinate transformation. Guha and Pradhan [4] formulated a unified integral theory for arbitrary inclination, in which the orders of polynomial representing the velocity and temperature profiles could be optimized. Table 5 shows that in the range of angles $15° \leqslant \gamma \leqslant 90°$ the results from the previous two methods are indicative of that from the present computations though the magnitudes of $\overline{Nu}$ obtained from the previous theoretical methods were slightly lower than the values obtained from the present computations. Table 5, however, shows that the values of $\overline{Nu}$ determined by the approach of Yu and Lin [33] and that determined by the unified integral method of Guha and Pradhan [4] are significantly different from the values of $\overline{Nu}$ determined in the present study in the range $0° \leqslant \gamma \leqslant 15°$. There are two reasons for this difference. The first reason (which is actually valid over the entire range from 0° to 90°) is that the present method solves the full Navier-Stokes equations in a carefully constructed computational domain and grid, the solutions being carried to high level of precision. The semi-analytical formulations use approximate equations. There is a second, more subtle reason for the greater deviations in the range $0° \leqslant \gamma \leqslant 15°$. In the present unified CFD approach, the length scale used in the analysis (for example in defining the Grashof number Gr_L) is taken to be the plate length L at all values of inclination angle γ. The same approach is also taken for the values shown in Table 5 for the entries corresponding to Refs. [4,33]. Eqs. (6)-(10) establish that the average Nusselt number, $\overline{Nu}$, computed through the present CFD solutions is directly indicative of the dependence of the overall heat transfer on the inclination angle. This may not be the case for the values of $\overline{Nu}$ computed through the approaches of Refs. [4,33]. We provide the following physical explanation. Ref. [1] established that, for a study of natural convection specifically on a horizontal plate, the most relevant length scale is $L/2$ (since convective boundary layers form on two halves of the plate with a plume in the middle, analytical theories based on semi-infinite assumption can be compared with CFD results up to a maximum limit of $L/2$). Since there is left-right symmetry in the fluid flow field and heat transfer characteristics in the CFD solution for the case of a horizontal plate, the average heat transfer coefficient $\overline{h}$ calculated over any one-half is the same as the arithmetic mean of the $\overline{h}$ values calculated over the left and right halves of the plate. This is not the case for the solutions given by similarity or integral theories which adopt the semi-infinite description. Suppose, these theories predict a total heat transfer rate of $Q_{L,semi-infinite}$ (defined as $\int_0^L q_x dx$) over a plate of length L (where the value of L is fixed by the same value of Gr_L used either in the theories or in the CFD simulation), then the actual total heat transfer rate should be calculated from $Q_{L,corrected} = 2Q_{L/2,semi-infinite}$ (where $Q_{L/2,semi-infinite}$ is the total heat transfer rate through half of the plate starting from the leading edge, given by $\int_0^{L/2} q_x dx$). Using the similarity theory [17], integral theories [18,4] or a more realistic theoretical treatment [1] for a horizontal plate, it can be shown that for the isothermal case q_x is given by $q_x = C/x^{2/5}$, where C is a function of Pr, $(T_w - T_\infty)$ and other properties, but C does not depend on x. Integration of this relation shows that $Q_{L,semi-infinite} = (5/3)CL^{3/5} = k(T_w - T_\infty)\overline{Nu}_{semi-infinite}$. Therefore, for a horizontal isothermal plate, the relation between the actual average Nusselt number and the average Nusselt number determined from similarity or integral theories may be established as follows:

$$\overline{Nu}_{corrected} = \frac{2Q_{L/2,semi-infinite}}{k(T_w - T_\infty)} = 2\left(\frac{1}{2}\right)^{3/5} \frac{Q_{L,semi-infinite}}{k(T_w - T_\infty)} = 2^{2/5}\overline{Nu}_{semi-infinite} \quad (18)$$

The correction incorporated in Eq. (18) accounts for the fact that boundary layers grow from both edges of a finite plate. Two further corrections are needed to the boundary layer approach [1]: edge-effect and the alteration of the thermo-fluid-dynamics due to the presence of lift-off point and the plume. Ref. [1] gives the details that heat transfer from the wall increases at the edges but decreases underneath the plume. So the combined effect of these two corrections produces a rather small change in the overall heat transfer rate. Applying the transformation derived above (i.e. Eq. (18)) to the CFD result for horizontal plate (Table 5), we obtain $12.4953/2^{2/5} = 9.4697$; then the present CFD result comes closer to the previous theoretical values [4,33]. For non-zero values of γ in the range $0^\circ < \gamma \leqslant 15^\circ$, however, the exact transformation is not known, and the correspondence between the previous theoretical values and present CFD results cannot be directly established.

Table 5 shows that the value of $\overline{Nu}$ determined by CFD is weakly dependent on inclination angle γ in the range $0^\circ \leqslant \gamma \leqslant 15^\circ$. However, Figs. 5, 8, 10 and 19 show that the flow field is a strong function of the inclination angle γ in the range $0^\circ \leqslant \gamma \leqslant 15^\circ$. In order to resolve this apparent paradox, the variation in local heat transfer rate q_x is plotted in Fig. 20 for various small values of γ. The curves have a distinctive shape; the physical reasons for such a shape can be explained as follows. The heat transfer rate is extremely high at the two edges because of the presence of the physical corners. As one moves inside from either of the two edges, the boundary layer thickness increases and the heat transfer rate gradually decreases in that direction. Each curve passes through a minimum point ($q_{x,\min}$) where the heat transfer rate is significantly lower than what could be expected from the general trend due to the growth of the boundary layer. The principal reason for the existence of the minimum heat flux point for near-horizontal orientations (where the buoyant plume forms within the heated side of the plate) is the reduced heat transfer underneath the plume (due to uplifting of the fluid as a result of confluence of two oppositely moving streams). The location ($\bar{x}_{q_{x,\min}}$) of the minimum point ($q_{x,\min}$) shifts from the centre of the plate for the horizontal position ($\gamma = 0^\circ$) to near the trailing edge as the inclination angle γ increases by a small amount. This sheds light on the difference in the local heat transfer characteristics over the plate length, in line with the difference in the fluid dynamics. However, the variation in q_x in the two sides of the minimum heat flux point is such that the area under the curve does not change significantly, thus making the overall heat transfer rather insensitive to the variation in γ in the range $0^\circ \leqslant \gamma \leqslant 15^\circ$.

Table 3 shows that even in the range $15^\circ \leqslant \gamma \leqslant 25^\circ$ the lift-off point occurs within the length of the plate ($\bar{x}_{lift-off} \leqslant 1$), though there is a significant change in $\overline{Nu}$ over this range of inclination angle. This is so because direct buoyancy has already established itself as the dominant mechanism (see Fig. 18).

Fig. 20 reveals another important feature of the local heat transfer characteristics. Each curve passes through a minimum point ($q_{x,\min}$) whose location ($\bar{x}_{q_{x,\min}}$) approximately coincides with that of the respective lift-off points; the correspondence may be studied from the data given in Table 3. Thus the lift-off phenomenon and the formation of the plume correspond to reduced heat transfer rate. This provides another qualitative consequence of the lift-off as well as another quantitative method of determining $\bar{x}_{lift-off}$ introduced in this paper. Except for the case of horizontal plate, the data in Table 3 show that the location of the minimum heat flux occurs a little ahead of the location of lift-off point determined from the velocity ratio v/u, as one travels from the mid-point of the plate toward its trailing (left) edge, i.e. $\bar{x}_{q_{x,\min}} < \bar{x}_{lift-off}$ in the interval $0^\circ < \gamma \leqslant 25^\circ$. Another subtle point is that the minimum heat flux point never quite reaches the trailing edge ($\bar{x}_{q_{x,\min}} = 0.9668$ at $\gamma = 25^\circ$) of the plate, even when the lift-off point does so. This is because of the finiteness of a real plate; the fluid flow field is such that the heat transfer rate is high both at the leading and the trailing edges of a finite plate. The variation of $\bar{x}_{lift-off}$ and $\bar{x}_{q_{x,\min}}$ with γ may be visualized from Fig. 21.

The values of the average Nusselt number determined from the present computations are plotted in Fig. 22 as a function of the inclination angle. It is found that as the inclination angle is increased gradually from the horizontal position, the value of $\overline{Nu}$ initially decreases slightly, passes through a minimum point and then onward increases continuously up to the vertical position of the plate. The rate of increase in $\overline{Nu}$ is large in the range $15^\circ \leqslant \gamma \leqslant 60^\circ$.

At fixed values of Gr_x (local Grashof number) and Pr, the unified integral theory [4] and the numerical results of Ref. [33] show a monotonic increase in the local Nusselt number Nu_x as inclination angle γ is progressively increased from 0° to 90°. $Nu_x = f(\gamma)$ were constructed from the present CFD simulations at two fixed x-locations on the plate surface between the leading (right) edge and mid-point of the plate (i.e. at two different values of Gr_x),

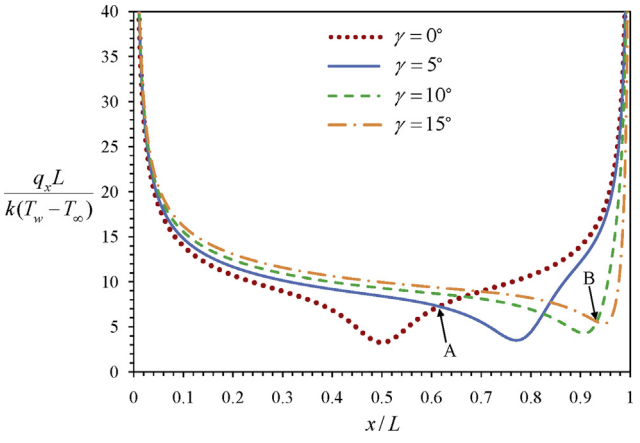

Fig. 20. Variation of non-dimensional local wall heat flux along the plate at various angles of inclination in the range $0^\circ \leqslant \gamma \leqslant 15^\circ$ (at $Gr_L = 10^6$, Pr = 0.7).

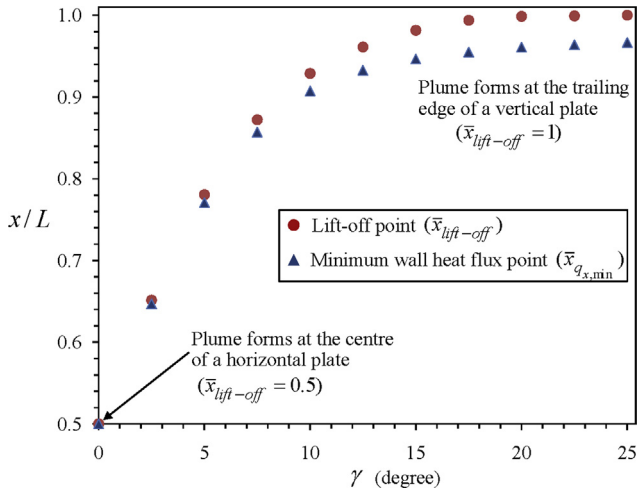

Fig. 21. Variation of locations of lift-off point and minimum wall heat flux point as a function of inclination angle (at $Gr_L = 10^6$, Pr = 0.7).

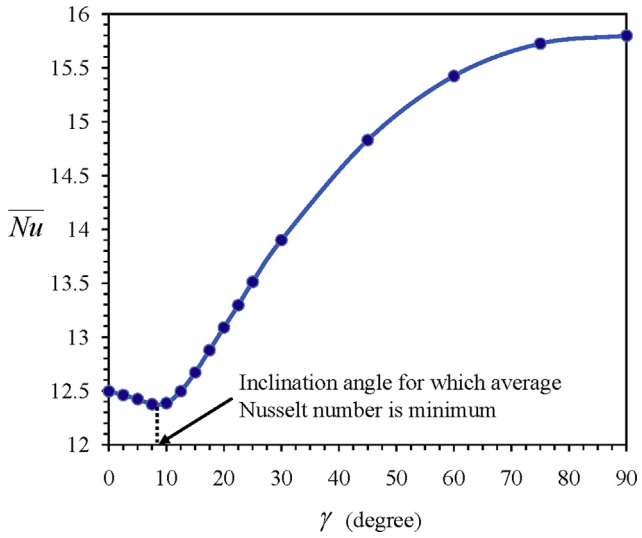

Fig. 22. Variation with angles of inclination of average Nusselt number determined from the present computations (at $Gr_L = 10^6$, Pr = 0.7).

and the same monotonicity is observed. The explanation for the existence of the minimum point in the $\overline{Nu} - \gamma$ curve (Fig. 22) thus seems to be the alteration of the thermo-fluid-dynamics due to the existence of the lift-off point (and the plume) arising from the finiteness of the plate. Between the leading (right) edge of the plate and the lift-off point, both indirect pressure difference and the direct buoyancy (which cause fluid motion parallel to the surface) act in the positive x-direction, and are thus additive in nature. Between the lift-off point and the trailing (left) edge of the plate, the direction of the direct buoyancy remains in the positive x-direction but the direction of the indirect pressure difference reverses over most of this region; the two forces thus largely oppose each other in this region (the discussion regarding Fig. 19 showed that the magnitude of $\partial p/\partial x$ can be relatively high in this region). Moreover, as γ increases, the lift-off point shifts towards the trailing (left) edge and the direct buoyancy term definitely increases because of the $\sin\gamma$ contribution. As a result of complex, non-linear interaction of the above effects, one obtains the local heat flux curves as shown in Fig. 20. It is found that the value of minimum heat flux ($q_{x,\min}$) increases as γ increases. Moreover, the curves on the two-sides of the lift-off point are asymmetric for non-zero values of γ. If we consider point A where the curves for $\gamma = 0^\circ$ and $\gamma = 5^\circ$ cross, it is found that the area between the two curves to the left of A is less than that to the right (i.e. $\overline{Nu}(\gamma = 5^\circ) < \overline{Nu}(\gamma = 0^\circ)$). The reverse is true for point B where the curves for $\gamma = 10^\circ$ and $\gamma = 15^\circ$ cross (i.e. $\overline{Nu}(\gamma = 15^\circ) > \overline{Nu}(\gamma = 10^\circ)$). This implies the existence of a minimum in the $\overline{Nu} - \gamma$ curve.

At the specific values of the Grashof number and Prandtl number, the minimum of $\overline{Nu}$ is found to occur (in Fig. 22) at $\gamma = 8.5^\circ$. This is reasonably close to the cross-over point depicted in Fig. 18, $\gamma_{cross-over} = 5.86^\circ$ being determined numerically in the present work. It is to be remembered that the magnitude of the force due to indirect pressure difference is equal to that due to direct buoyancy at $\gamma_{cross-over}$. Thus another important new conclusion is established in the present work that an increase in the inclination angle γ tends to decrease $\overline{Nu}$ when the major mechanism of natural convection is indirect pressure difference and the same tends to increase $\overline{Nu}$ when the major mechanism of natural convection is direct buoyancy.

5. Conclusion

The present study aims to develop, by invoking the power of computational fluid dynamics, a thorough understanding of the thermo-fluid-dynamics of natural convective flows adjacent to isothermally heated plates at arbitrary inclination. The agreement between the experiments and present computations (Table 4), in the values of both local Nusselt number Nu_x and average Nusselt number $\overline{Nu}$, over the range of Rayleigh number and plate inclination angle (γ) is excellent, giving confidence in the physical conclusions made here. As a result of the insight gained from the present CFD solutions for finite plates, it has been possible to put in perspective (see the discussion regarding Table 5) the Nusselt numbers determined from previous theoretical approaches which use several assumptions and approximations such as semi-infinite plate, boundary layer equations, non-physical boundary conditions and absence of any plume.

The goal of this work, however, is not merely the calculation of the Nusselt number. It provides fundamental physical insight through a comprehensive analysis of the behaviour of the contours of velocity, temperature and pressure as a function of inclination angle over the entire range from the vertical ($\gamma = 90^\circ$) to the horizontal ($\gamma = 0^\circ$). In particular, this paper documents, for the first time, qualitative and quantitative behaviour of the lift-off point at which the natural convective boundary layer converts into a free plume. The fluid dynamics and heat transfer in the neighbourhood of the lift-off point are analysed in detail (Sections 4.3 and 4.4). Similarly, the details of the spatial evolution of the velocity profile and temperature profile in the plume as a function of the inclination angle of the plate are determined for the first time (Section 4.2). The role of indirect pressure difference is quantified (Figs 10, 11, 18 and 19), and it is shown how the relative importance of indirect pressure difference and direct buoyancy, as mechanisms of natural convection, changes as the inclination angle is gradually altered from the horizontal to the vertical. Through detailed computation (and representation, Section 4.1) of the velocity, temperature and pressure fields at small intervals of the inclination angle in the range $0^\circ \leqslant \gamma \leqslant 15^\circ$ the subtle and complex thermo-fluid-dynamics for near-horizontal orientations is revealed.

The plume forms above the trailing edge for the vertical configuration, whereas it forms above the middle of the plate for the horizontal. For all inclination angles, the plume eventually aligns with the negative g direction. Fig. 15 shows that the maximum value in V_Y decreases and its location shifts toward the left (i.e. occurs at a greater value of negative X/L) as the inclination angle decreases. This trend, however, must reverse at a certain value of inclination angle $\gamma_{reversal}$, because we know from the discussion in Section 4.2.3 for the horizontal plate that the maximum occurs above the middle of the plate (i.e. at $X/L = 0.5$), which is situated to the right side of the adopted origin. As γ is progressively decreased below $\gamma_{reversal}$ up to $\gamma = 0^\circ$, the value of maximum V_Y decreases slightly and the location of the maximum moves to the right. This rightward movement of the location of the maximum is a strong function of γ in the range $0^\circ \leqslant \gamma \leqslant 15^\circ$.

Although Figs. 5, 8, 10 and 19 show that the flow field is a strong function of the inclination angle γ in the range $0^\circ \leqslant \gamma \leqslant 15^\circ$, Table 5 shows that the value of $\overline{Nu}$ determined by CFD is weakly dependent on inclination angle γ in the same range. This apparent paradox is resolved here by analysing the variations in local heat transfer rate q_x (Fig. 20) for various small values of γ. The strong dependence of the lift-off distance $\bar{x}_{lift-off}$ on γ, and the correspondence between $\bar{x}_{lift-off}$ and $\bar{x}_{q_{x,\min}}$ (the location of the minimum heat transfer point) are depicted in Fig. 21.

It is established that as the inclination angle is increased gradually from the horizontal position, the value of $\overline{Nu}$ initially decreases slightly, passes through a minimum point and then onward increases continuously up to the vertical position of the plate (Fig. 22). The information is of fundamental as well as of engineering importance since $\overline{Nu}$ is a measure of the overall heat transfer ($\overline{Nu} = [1/k(T_w - T_\infty)] \int_0^L q_x dx$) for a plate of given length (and given temperature difference). The rate of increase in $\overline{Nu}$ is large in the range $15^\circ \leqslant \gamma \leqslant 60^\circ$. It is further shown that the angle at which the minimum $\overline{Nu}$ occurs is related to the angle $\gamma_{cross-over}$ at which the magnitude of the force due to indirect pressure difference is equal to that due to direct buoyancy. Thus another important new conclusion is established in the present work that an increase in the inclination angle γ tends to decrease $\overline{Nu}$ when the major mechanism of natural convection is indirect pressure difference and the same tends to increase $\overline{Nu}$ when the major mechanism of natural convection is direct buoyancy.

Conflict of interest

We wish to confirm that there are no known conflicts of interest associated with this publication.

References

[1] A. Guha, S. Sengupta, Effects of finiteness on the thermo-fluid-dynamics of natural convection above horizontal plates, Phys. Fluids 28 (6) (2016), 063603:1–29.
[2] A. Guha, S. Nayek, Thermo-fluid-dynamics of natural convection around a heated vertical plate with a critical assessment of the standard similarity theory, Phys. Fluids 29 (10) (2017), 103607:1–17.
[3] A. Guha, S. Sengupta, Non-linear interaction of buoyancy with von Kármán's swirling flow in mixed convection above a heated rotating disc, Int. J. Heat Mass Transfer 108 (Part A) (2017) 402–416.
[4] A. Guha, K. Pradhan, A unified integral theory of laminar natural convection over surfaces at arbitrary inclination from horizontal to vertical, Int. J. Therm. Sci. 111 (2016) 475–490.
[5] S.A.M. Said, M.A. Habib, H.M. Badr, S. Anwar, Turbulent natural convection between inclined isothermal plates, Comput. Fluids 34 (9) (2005) 1025–1039.
[6] P. Ganesan, G. Palani, Natural convection effects on impulsively started inclined plate with heat and mass transfer, Heat Mass Transfer 39 (4) (2003) 277–283.
[7] L.C. Burmeister, Convective Heat Transfer, second ed., John Wiley & Sons, New York, USA, 1993.
[8] W.M. Kays, M.E. Crawford, Convective Heat and Mass Transfer, third ed., McGraw-Hill, New York, USA, 1993.
[9] J.P. Holman, Heat Transfer, ninth ed., Tata McGraw-Hill, New Delhi, India, 2008.
[10] H. Schlichting, K. Gersten, Boundary-Layer Theory, eighth ed., Springer, New Delhi, India, 2004.
[11] O.A. Saunders, Natural convection in liquids, Proc. Roy. Soc. A 172 (1939) 55–71.
[12] R.J. Goldstein, E.R.G. Eckert, The steady and transient free convection boundary layer on a uniformly heated vertical plate, Int. J. Heat Mass Transfer 1 (2–3) (1959) 208–218.
[13] J. Gryzagoridis, Natural convection from a vertical flat plate in the low Grashof number range, Int. J. Heat Mass Transfer 14 (1) (1971) 162–165.
[14] M. Fishenden, O.A. Saunders, An Introduction to Heat Transfer, Oxford University Press, London, 1950.
[15] S. Ostrach, An analysis of laminar free convection flow and heat transfer about a flat plate parallel to the direction of the governing body force, NACA Report 1111, 1953.
[16] E.M. Sparrow, Laminar free convection on a vertical plate with prescribed non uniform wall heat flux or prescribed non uniform wall temperature, NACA Tech. Note 3508 (1955) 1–34.
[17] S. Samanta, A. Guha, A similarity theory for natural convection from a horizontal plate for prescribed heat flux or wall temperature, Int. J. Heat Mass Transfer 55 (13–14) (2012) 3857–3868.
[18] A. Guha, S. Samanta, Closed-form analytical solutions for laminar natural convection on horizontal plates, ASME J. Heat Transfer 135 (10) (2013), 102501:1–9.
[19] Z. Rotem, L. Claassen, Natural convection above unconfined horizontal surfaces, J. Fluid Mech. 39 (1) (1969) 173–192.
[20] K. Stewartson, On the free convection from a horizontal plate, Z. Angew. Math. Phys.ZAMP 9 (3) (1958) 276–282.
[21] W.N. Gill, D.W. Zeh, E. Del Casal, Free convection on a horizontal plate, Z. Angew. Math. Phys. ZAMP 16 (4) (1965) 539–541.
[22] A. Guha, K. Pradhan, Natural convection of non-Newtonian power-law fluids on a horizontal plate, Int. J. Heat Mass Transfer 70 (2014) 930–938.
[23] K. Pradhan, S. Samanta, A. Guha, Natural convective boundary layer flow of nanofluids above an isothermal horizontal plate, ASME J. Heat Transfer 136 (10) (2014), 102501:1–9.
[24] K. Pradhan, A. Guha, Natural convection above a horizontal plate in a nanofluid-saturated porous medium with or without a magnetic field, J. Porous Media 18 (6) (2015) 613–628.
[25] K. Pradhan, A. Guha, CFD solutions for magnetohydrodynamic natural convection over horizontal and vertical surfaces, J. Mol. Liquids 236 (2017) 465–476.
[26] B. Gebhart, Y. Jaluria, R.L. Mahajan, B. Sammakia, Buoyancy-induced Flows and Transport, first ed., Hemisphere Publishing Corporation, USA, 1988.
[27] T.S. Chen, H.C. Tien, B.F. Armaly, Natural convection on horizontal, inclined and vertical plates with variable surface temperature or heat flux, Int. J. Heat Mass Transfer 29 (10) (1986) 1465–1478.
[28] S. Samanta, A. Guha, Similarity theory for forced convection over horizontal plates, J. Thermophys. Heat Transfer 27 (3) (2013) 506–514.
[29] S.M. Ghiaasiaan, Convective Heat and Mass Transfer, second ed., CRC Press, 2018.
[30] B.R. Rich, An investigation of heat transfer from an inclined flat plate in free convection, ASME J. Heat Transfer 75 (1953) 485–499.
[31] P. Sang-Urai, Investigation of free convection heat transfer from an inclined flat plate, MS Thesis, University of Missouri-Rolla, 1969.
[32] G.C. Vliet, Natural convection local heat transfer on constant heat flux inclined surfaces, ASME J. Heat Transfer 91 (4) (1969) 511–516.
[33] W.S. Yu, H.T. Lin, Free convection heat transfer from an isothermal plate with arbitrary inclination, Wärme-und Stoffübertragung 23 (4) (1988) 203–211.
[34] S.C. Saha, J.C. Patterson, C. Lei, Natural convection boundary-layer adjacent to an inclined flat plate subject to sudden and ramp heating, Int. J. Therm. Sci. 49 (9) (2010) 1600–1612.
[35] M. Corcione, E. Habib, A. Campo, Natural convection from inclined plates to gases and liquids when both sides are uniformly heated at the same temperature, Int. J. Therm. Sci. 50 (8) (2011) 1405–1416.
[36] B. Gebhart, Effect of viscous dissipation in natural convection, J. Fluid Mech. 14 (2) (1962) 225–232.
[37] Ansys Inc., ANSYS FLUENT 12.0 User's Guide, 2009.
[38] A. Guha, S. Samanta, Effect of thermophoresis on the motion of aerosol particles in natural convective flow on horizontal plates, Int. J. Heat Mass Transfer 68 (2014) 42–50.
[39] A. Guha, S. Samanta, Effect of thermophoresis and its mathematical models on the transport and deposition of aerosol particles in natural convective flow on vertical and horizontal plates, J. Aerosol Sci. 77 (2014) 85–101.
[40] J.R. Lloyd, E.M. Sparrow, E.R.G. Eckert, Laminar, transition and turbulent natural convection adjacent to inclined and vertical surfaces, Int. J. Heat Mass Transfer 15 (3) (1972) 457–473.
[41] P.E. Dimotakis, The mixing transition in turbulent flows, J. Fluid Mech. 409 (2000) 69–98.
[42] Y. Mei, A. Guha, Implicit numerical simulation of transonic flow through turbine cascades on unstructured grids, Proc. Inst. Mech. Eng. Part A 219 (1) (2005) 35–47.
[43] A. Guha, J.B. Young, Time-marching prediction of unsteady condensation phenomena due to supercritical heat addition, in: Turbomachinery: Latest Developments in a Changing Scene, Institution of Mechanical Engineers, London, UK, 1991, ISBN: 0852987617, pp. 167-177.
[44] A. Guha, Thermal choking due to nonequilibrium condensation, ASME J. Fluids Eng. 116 (3) (1994) 599–604.
[45] R.J. Whittaker, J.R. Lister, Steady axisymmetric creeping plumes above a planar boundary. Part 2. A distributed source, J. Fluid Mech. 567 (2006) 379–397.